



1 Importance of Dry Deposition Parameterization Choice in Global 2 Simulations of Surface Ozone

3 Anthony Y.H. Wong¹, Jeffrey A. Geddes¹, Amos P.K. Tai^{2,3}, Sam J. Silva⁴

4 ¹Department of Earth and Environment, Boston University, Boston, MA, USA

5 ²Earth System Science Programme, Faculty of Science, The Chinese University of Hong Kong, Hong Kong

6 ³Institute of Energy, Environment and Sustainability, and State Key Laboratory of Agrobiotechnology, The Chinese University
7 of Hong Kong, Hong Kong

8 ⁴Department of Civil and Environmental Engineering, Massachusetts Institute of Technology, Cambridge, MA, USA

9 Correspondence to: Jeffrey A. Geddes (jgeddes@bu.edu)

10 **Abstract.** Dry deposition is the second largest sink of tropospheric ozone. Increasing evidence has shown that ozone dry
11 deposition actively links meteorology and hydrology with ozone air quality. However, there is little systematic investigation
12 on the performance of different ozone dry deposition parameterizations at the global scale, and how parameterization choice
13 can impact surface ozone simulations. Here we present the results of the first global, multi-decade modelling and evaluation
14 of ozone dry deposition velocity (v_d) using multiple ozone dry deposition parameterizations. We use consistent assimilated
15 meteorology and satellite-derived leaf area index (LAI) to simulate v_d over 1982-2011 driven by four sets of ozone dry
16 deposition parametrization that are representative of the current approaches of global ozone dry deposition modelling, such
17 that the differences in simulated v_d are entirely due to differences in deposition model structures. In addition, we use the surface
18 ozone sensitivity to v_d predicted by a chemical transport model to estimate the impact of mean and variability of ozone dry
19 deposition velocity on surface ozone. Our estimated v_d from four different parameterizations are evaluated against field
20 observations, and while performance varies considerably by land cover types, our results suggest that none of the
21 parameterizations are universally better than the others. Discrepancy in simulated mean v_d among the parameterizations is
22 estimated to cause 2 to 5 ppbv of discrepancy in surface ozone in the Northern Hemisphere (NH) and up to 8 ppbv in tropical
23 rainforest in July, and up to 8 ppbv in tropical rainforests and seasonally dry tropical forests in Indochina in December.
24 Parameterization-specific biases based on individual land cover type and hydroclimate are found to be the two main drivers of
25 such discrepancies. We find statistically significant trends in the multiannual time series of simulated July daytime v_d in all
26 parameterizations, driven by warming and drying (southern Amazonia, southern African savannah and Mongolia) or greening
27 (high latitudes). The trends in July daytime v_d is estimated to be 1 % yr⁻¹ and leads to up to 3 ppbv of surface ozone changes
28 over 1982-2011. The interannual coefficient of variation (CV) of July daytime mean v_d in NH is found to be 5%-15%, with
29 spatial distribution that varies with the dry deposition parameterization. Our sensitivity simulations suggest this can contribute
30 between 0.5 to 2 ppbv to interannual variability (IAV) in surface ozone, but all models tend to underestimate interannual CV
31 when compared to long-term ozone flux observations. We also find that IAV in some dry deposition parameterizations are
32 more sensitive to LAI while others are more sensitive to climate. Comparisons with other published estimates of the IAV of



33 background ozone confirm that ozone dry deposition can be an important part of natural surface ozone variability. Our results
34 demonstrate the importance of ozone dry deposition parameterization choice on surface ozone modelling, and the impact of
35 IAV of v_d on surface ozone, thus making a strong case for further measurement, evaluation and model-data integration of
36 ozone dry deposition on different spatiotemporal scales.

37 1 Introduction

38 Surface ozone (O_3) is one of the major air pollutants that poses serious threats to human health (Jerrett et al., 2009) and plant
39 productivity (Ainsworth et al., 2012; Reich, 1987; Wittig et al., 2007). Ozone exerts additional pressure on global food security
40 and public health by damaging agricultural ecosystems and reducing crop yields (Avnery et al., 2011; McGrath et al., 2015;
41 Tai et al., 2014). Dry deposition, by which atmospheric constituents are removed from the atmosphere and transferred to the
42 Earth's surface through turbulent transport or gravitational settling, is the second-largest and terminal sink of tropospheric O_3
43 (Wild, 2007). Terrestrial ecosystems are particularly efficient at removing O_3 via dry deposition through stomatal uptake and
44 other non-stomatal pathways (Wesely and Hicks, 2000) (e.g., cuticle, soil, reaction with biogenic volatile organic compounds
45 (BVOCs) (Fares et al., 2010; Wolfe et al., 2011). Meanwhile, stomatal uptake of O_3 inflicts damage on plants by initiating
46 reactions that impair their photosynthetic and stomatal regulatory capacity (Hoshika et al., 2014; Lombardozzi et al., 2012;
47 Reich, 1987). Widespread plant damage has the potential to alter the global water cycle (Lombardozzi et al., 2015) and suppress
48 the land carbon sink (Sitch et al., 2007), as well as to generate a cascade of feedbacks that affect atmospheric composition
49 including ozone itself (Sadiq et al., 2017; Zhou et al., 2018). Ozone dry deposition is therefore key in understanding how
50 meteorology (Kavassalis and Murphy, 2017), climate, and land cover change (Fu and Tai, 2015; Ganzeveld et al., 2010; Geddes
51 et al., 2016; Heald and Geddes, 2016; Sadiq et al., 2017; Sanderson et al., 2007; Young et al., 2013) can affect air quality and
52 atmospheric chemistry at large.

53
54 Analogous to other surface-atmosphere exchange processes (e.g., sensible and latent heat flux), O_3 dry deposition flux (F_{O_3})
55 is often expressed as the product of ambient O_3 concentrations at the surface ($[O_3]$) and a transfer coefficient (dry deposition
56 velocity, v_d) that describes the efficiency of transport (and removal) to the surface from the measurement height:

$$57 F_{O_3} = [O_3]v_d \quad (1)$$

58 Also analogous to other surface fluxes, F_{O_3} , $[O_3]$, and hence v_d can be directly measured by the eddy covariance (EC) method
59 (e.g. Fares et al., 2014; Gerosa et al., 2005; Lamaud et al., 2002; Munger et al., 1996; Rannik et al., 2012) with random
60 uncertainty of about 20% (Keronen et al., 2003; Muller et al., 2010). Apart from EC, F_{O_3} and v_d can also be estimated from
61 the vertical profile of O_3 by exploiting flux-gradient relationship (Foken, 2006) (termed the gradient method, GM) (e.g. Gerosa
62 et al., 2017; Wu et al., 2016, 2015). A recent review (Silva and Heald, 2018) has compiled 75 sets of ozone deposition
63 measurement from the EC and GM methods across different seasons and land cover types over the past 30 years.

64



65 At the site level, ozone dry deposition over various terrestrial ecosystems can be simulated comprehensively by 1-D chemical
66 transport models (Ashworth et al., 2015; Wolfe et al., 2011; Zhou et al., 2017), which are able to account for vertical gradients
67 inside the canopy environment, and gas-phase reaction with BVOCs in addition to surface sinks. Regional and global models,
68 which lack the fine-scale information (e.g. vertical structure of canopy, in-canopy BVOCs emissions) and horizontal resolution
69 for resolving the plant canopy in such detail, instead rely on parameterizing v_d as a network of resistances, which account for
70 the effects of turbulent mixing via aerodynamic (R_a), molecular diffusion via quasi-laminar sublayer resistances (R_b), and
71 surface sinks via surface resistance (R_c):

72
$$v_d = \frac{1}{R_a + R_b + R_c} \quad (2)$$

73

74 A diverse set of parameterizations of ozone dry deposition are available and used in different models and monitoring networks.
75 Examples include the Wesely parameterization (1989) and modified versions of it (e.g. Wang et al., 1998), the Zhang et al.
76 parameterization (Zhang et al., 2003), the Deposition of O₃ for Stomatal Exchange model (Emberson et al., 2000; Simpson et
77 al., 2012), and the Clean Air Status and Trends Network (CASTNET) deposition estimates (Meyers et al., 1998). The
78 calculation of R_a and R_b across these parameterizations often follow a standard formulation from micrometeorology (Foken,
79 2006; Wesely and Hicks, 1977, 2000; Wu et al., 2011) and thus does not vary significantly. The main difference between the
80 ozone dry deposition parameterizations lies on the surface resistance R_c . This resistance includes stomatal resistance (R_s),
81 which can be computed by a Jarvis-type multiplicative algorithm (Jarvis, 1976) where R_s is the product of its minimum value
82 and a series of response functions to individual environmental conditions. Such conditions typically include air temperature
83 (T), photosynthetically available radiation (PAR), vapour pressure deficit (VPD) and soil moisture (θ), with varying complexity
84 and functional forms.

85

86 An advance of these efforts includes harmonizing R_s with that computed by land surface models (Ran et al., 2017a; Val Martin
87 et al., 2014), which calculate R_s by coupled photosynthesis-stomatal conductance (A_n-g_s) models (Ball et al., 1987; Collatz et
88 al., 1992, 1991). Such coupling should theoretically give a more realistic account of ecophysiological controls on R_s . Indeed,
89 it has been shown that the above approach may better simulate v_d than the multiplicative algorithms that only considers the
90 effects T and PAR (Val Martin et al., 2014; Wu et al., 2011). The non-stomatal part of R_c often consists of cuticular (R_{cut}),
91 ground (R_g) and other miscellaneous types of resistances (e.g., lower canopy resistance (R_{lc}) in Wesely (1989)). Due to very
92 limited measurements and mechanistic understanding towards non-stomatal deposition, non-stomatal resistances are often
93 constants (e.g., R_g) or simply scaled with leaf area index (LAI) (e.g., R_{cut}) (Simpson et al., 2012; Wang et al., 1998; Wesely,
94 1989), while some of the parameterizations (Zhang et al., 2003; Zhou et al., 2017) incorporate the observation of enhanced
95 cuticular O₃ uptake under leaf surface wetness (Altimir et al., 2006; Potier et al., 2015, 2017; Sun et al., 2016).

96



97 Various efforts have been made to evaluate and assess the uncertainty in modelling ozone dry deposition using field
98 measurements. Hardacre et al. (2015) evaluate the performance of simulated monthly mean v_d and F_{O_3} by 15 chemical transport
99 models (CTM) from the Task Force on Hemispheric Transport of Air Pollutant (TF HTAP) against seven long-term site
100 measurements, 15 short-term site measurements, and modelled v_d from 96 CASTNET sites. This work found that the seasonal
101 cycle is well-simulated across models, while demonstrating that the difference in land cover classification is the main source
102 of discrepancy between models. In this case, most of the models in TF HTAP use the same class of dry deposition
103 parameterization (Wang et al., 1998; Wesely, 1989), so a global evaluation of *different* deposition parameterizations was not
104 possible. Also, the focus in this intercomparison study was on seasonal, but not other (e.g. diurnal, daily, interannual)
105 timescales. Using an extended set of measurements, Silva and Heald (2018) evaluate the v_d output from the Wang et al. (1998)
106 parameterization used by the GEOS-Chem chemical transport model. They show that diurnal and seasonal cycles are generally
107 well-captured, while the daily variability is not well-simulated. They find that differences in land type and LAI, rather than
108 meteorology, are the main reason behind model-observation discrepancy at the seasonal scale, and eliminating this model bias
109 results in up to 15% change in surface O_3 . This study is also limited to a single parameterization. Using parameterizations that
110 are explicitly sensitive to other environmental variables (e.g. Simpson et al., 2012; Zhang et al., 2003) could conceivably lead
111 to different conclusions.

112

113 Other efforts have been made to compare the performance of different parameterizations. Centoni (2017) find that two different
114 dry deposition parameterizations, Wesely (1989) versus Zhang et al. (2003), implemented in the same chemistry-aerosol model
115 (United Kingdom Chemistry Aerosol model, UKMA), result in up to a 20% difference in simulated surface O_3 concentration.
116 This study demonstrates that uncertainty in v_d can have large potential effect on surface O_3 simulation. Wu et al. (2018)
117 compare v_d simulated by five North-American dry deposition parametrizations to a long-term observational record at a single
118 mixed forest in southern Canada, and find a large spread between the simulated v_d , with no single parameterization uniformly
119 outperforming others. They further acknowledge that as each parameterization is developed with its own set of limited
120 observations, it is natural that their performance can vary considerably under different environments, and advocate for an
121 “ensemble” approach to dry deposition modelling. This highlights the importance of parameterization choice as a key source
122 of uncertainty in modelling ozone dry deposition. Meanwhile, in another evaluation at a single site, Clifton et al. (2017) show
123 that the GEOS-Chem parameterization largely underestimates the interannual variability (IAV) of v_d in Harvard Forest based
124 on the measurement from 1990 to 2000, although they were unable to conclude how the IAV of v_d may contribute to the IAV
125 of O_3 .

126

127 These developments have made a substantial contribution to our understanding of the importance of O_3 dry deposition in
128 atmospheric chemistry models. Still, pertinent questions remain about the impact of dry deposition model physics on
129 simulations of the global distribution of ozone and its long-term variability. Here, we build on previous works by posing and
130 answering the following questions:



131 1) How does the global distribution of mean v_d vary with different dry deposition parameterizations, and what drives the
132 discrepancies among them? How much might the choice of deposition parameterization affect spatial distribution of
133 surface ozone concentration simulated by a chemical transport model?

134 2) How are the IAV and long-term trends of v_d different across deposition parameterizations, and what drives the
135 discrepancies among them? Do they potentially contribute different predictions of the long-term temporal variability
136 in surface ozone?

137 The answers to such question could have important consequences on our ability to predict long-term changes in atmospheric
138 O_3 concentrations as a function of changing climate and land cover characteristics. In general, there is a high computational
139 cost to thorough and large-scale evaluations of different dry deposition parameterizations embedded in CTMs. In this study,
140 we explore these questions using a strategy that combines an offline dry deposition modelling framework incorporating long-
141 term assimilated meteorological and land surface remote sensing data, in combination with a set of CTM sensitivity
142 simulations.

143 2 Method

144 2.1 Dry deposition parameterization

145 A detailed description of the common dry deposition parameterizations we explore can be found in Wu et al. (2018). Here we
146 consider several “big-leaf” models commonly used by global chemical transport models. More complex multilayer models
147 require the vertical profiles of leaf area density for different biomes which are generally not available for regional and global
148 models. From the wide range of literature on dry deposition studies, we observe that R_s is commonly modelled through one of
149 the following approaches:

- 150 1) Multiplicative algorithm that considers the effects of LAI, temperature and radiation (Wang et al., 1998).
- 151 2) Multiplicative algorithm that considers the effects of LAI, temperature, radiation and water stress (e.g. Meyers et al.,
152 1998; Pleim and Ran, 2011; Simpson et al., 2012; Zhang et al., 2003).
- 153 3) Coupled A_n - g_s model, which exploit the strong empirical relationship between photosynthesis (A_n) and stomatal
154 conductance (g_s) and to simulate A_n and $g_s = 1/R_s$ simultaneously (e.g. Ran et al., 2017b; Val Martin et al., 2014).

155 Similarly, their functional dependence of non-stomatal surface resistances can be classified into two classes:

- 156 1) Mainly scaling with LAI, with in-canopy aerodynamics parameterized as function of friction velocity (u_*) or radiation
157 (Meyers et al., 1998; Simpson et al., 2012; Wang et al., 1998)
- 158 2) Additional dependence of cuticular resistance on relative humidity (Pleim and Ran, 2011; Zhang et al., 2003)

159

160 With these considerations, we identify four common parameterizations that are representative of the types of approaches
161 described above:



- 162 1) The version of Wesely (1989) with the modification from Wang et al. (1998) (hereafter referred to as W98), which is
163 used extensively in global CTMs (Hardacre et al., 2015) and comprehensively discussed by Silva and Heald (2018).
164 This represents Type 1 in both stomatal and non-stomatal parametrizations.
- 165 2) The Zhang et al. (2003) parameterization (hereafter referred to as Z03), which is used in many North American air
166 quality modelling studies (e.g. Huang et al., 2016; Kharol et al., 2018) and Canadian Air and Precipitation Monitoring
167 Network (CAPMoN) (e.g. Zhang et al., 2009). This represents Type 2 in both stomatal and non-stomatal
168 parameterizations
- 169 3) W89 with R_s calculated from a widely-used coupled A_n - g_s model, the Ball-Berry model (hereafter referred to as
170 W98_BB) (Ball et al., 1987; Collatz et al., 1992, 1991), which is similar to that proposed by Val Martin et al. (2014).
171 This represents Type 3 in stomatal and Type 1 in non-stomatal parametrization.
- 172 4) Z03 with the Ball-Berry model (Z03_BB), which is comparable to the configuration in Centoni (2017). This
173 represents Type 3 in stomatal and Type 2 in non-stomatal parametrization.

174

175 Another important consideration in choosing Z03 and W98 is that they both have open-source parameters for all major land
176 types over the globe, making them widely applicable in global modelling. We extract the source code (Wang et al., 1998) and
177 parameters (Baldocchi et al., 1987; Jacob et al., 1992; Jacob and Wofsy, 1990; Wesely, 1989) of W98 from GEOS-Chem CTM
178 (http://wiki.seas.harvard.edu/geos-chem/index.php/Dry_deposition). The source code of Z03 are obtained through personal
179 communication with Zhiyong Wu and Leiming Zhang, which follows the series of papers that described the development and
180 formalism of the parameterization (Brook et al., 1999; Zhang et al., 2001, 2002, 2003). The Ball-Berry A_n - g_s model (Ball et
181 al., 1987; Collatz et al., 1992, 1991; Farquhar et al., 1980) and its solver are largely based on the algorithm of CLM
182 (Community Land Model) version 4.5 (Oleson et al., 2013), which is numerically stable (Sun et al., 2012). Since R_c typically
183 dominates the deposition velocity of O_3 (Fares et al., 2010; Wu et al., 2018), we use identical formulae of R_a and R_b (Paulson,
184 1970; Wesely and Hicks, 1977) for each individual parameterizations, allowing us to focus our analysis on differences in
185 parameterizations of R_c alone. Table A1 gives a brief description on the formalism of each of the dry deposition
186 parameterizations.

187 2.2 Dry deposition model configuration, inputs, and simulation

188 The above parameterizations are re-implemented in R language (R core team, 2017) in the modeling framework of the
189 Terrestrial Ecosystem Model in R (<http://www.cuhk.edu.hk/sci/essc/tgabi/tools.html>), and driven by gridded surface
190 meteorology and land surface data sets. The meteorological forcing chosen for this study is the Modern-Era Retrospective
191 Analysis for Research and Application-2 (MERRA-2) (Gelaro et al., 2017), an assimilated meteorological product at hourly
192 time resolution spanning from 1980 to present day. MERRA-2 contains all the required surface meteorological fields except
193 VPD and RH , which can be readily computed from T , specific humidity (q) and surface air pressure (P). We use the CLM land
194 surface dataset (Lawrence and Chase, 2007), which contains information for land cover, per-grid cell coverage of each plant



195 functional type (PFT), PFT-specific LAI and soil property. CLM land types are mapped to the land type of W98 following
196 Geddes et al. (2016). The mapping between CLM and Z03 land types are given in Table A2. Other relevant vegetation and
197 soil parameters (e.g. leaf physiological and soil hydraulic constants) are also imported from CLM 4.5 (Oleson et al., 2013),
198 while land cover specific z_0 values follow Geddes et al. (2016).

199

200 As the IAV of LAI could be an important factor in simulating v_d , the widely-used third generation Global Inventory Modelling
201 and Mapping Studies Leaf Area Index product (GIMMS LAI3g, abbreviated as LAI3g in this paper) (Zhu et al., 2013), which
202 is a global time series of LAI with 15-day temporal frequency and 1/12 degree spatial resolution spanning from late 1981 to
203 2011, is incorporated in this study. We use this data set to derive interannual scaling factors that can be applied to the baseline
204 CLM-derived LAI (Lawrence and Chase, 2007). All the input data are aggregated into horizontal resolution of $2^\circ \times 2.5^\circ$ to align
205 with the CTM sensitivity simulation described in next sub-section. To represent sub-grid land cover heterogeneity, grid cell-
206 level v_d is calculated as the sum of v_d over all sub-grid land types weighted by their percentage coverage in the grid cell (a.k.a
207 tiling or mosaic approach, e.g. Li et al., 2013). This reduces the information loss when land surface data is aggregated to
208 coarser spatial resolution, and allows us to retain PFT-specific results for each grid box in the offline dry deposition
209 simulations.

210

211 We run three sets of 30-years (1982-2011) simulations with the deposition parameterizations to investigate the how v_d
212 simulated by different parameterizations responds to different environmental factors over multiple decades. The settings of the
213 simulations are summarized in Table 1. The first set, [Clim], focuses on meteorological variability alone, driven by MERRA-
214 2 meteorology and a multiyear (constant) mean annual cycle of LAI derived from LAI3g. The second set, [Clim+LAI],
215 combines the effects of meteorology and IAV in LAI, driven by the same MERRA-2 meteorology plus the LAI time series
216 from LAI3g. As the increase atmospheric CO_2 level over multidecadal timescales may lead to significant reduction in g_s , as
217 plants tend to conserve water (e.g. Franks et al., 2013; Rigden and Salvucci, 2017), we introduce the third set of simulation,
218 [Clim+LAI+ CO_2], which is driven by varying meteorology and LAI, plus the annual mean atmospheric CO_2 level measured
219 in Mauna Loa (Keeling et al., 2001) (for the first two sets of simulations, atmospheric CO_2 concentration held constant at 390
220 ppm). Since W98 and Z03 do not respond to changes in CO_2 level, only W98_BB and Z03_BB are run with [Clim+LAI+ CO_2]
221 to evaluate this impact. We focus on the daytime (solar elevation angle $> 20^\circ$) v_d , as both v_d and surface O_3 concentration
222 typically peak around this time. We calculate monthly means, filtering out the grid cells with monthly total daytime < 100
223 hours, which would be an indication of dormant biosphere.

224

225 In summary, we present for the first time a unique set of global dry deposition velocity predictions over the last 30 years driven
226 by identical meteorology and land cover, so that discrepancies (in space and time) among the predicted v_d are a result
227 specifically of dry deposition parameterizations alone.



228 2.3 Chemical transport model sensitivity experiments

229 We quantify the sensitivity of surface O₃ to variations in v_d using a global 3D CTM, GEOS-Chem version 11.01 (Bey et al.,
230 2001), which includes comprehensive HO_x-NO_x-VOC-O₃-BrO_x chemical mechanisms (Mao et al., 2013) and is widely used
231 to study tropospheric ozone (e.g. Hu et al., 2017; Travis et al., 2016; Zhang et al., 2010). The model is driven by the assimilated
232 meteorological data from the GEOS-FP (Forward Processing) Atmospheric Data Assimilation System (GEOS-5 ADAS)
233 (Rienecker et al., 2008), which is jointly developed by National Centers for Environmental Prediction (NCEP) and the Global
234 Modelling and Assimilation Office (GMAO). The model is run with a horizontal resolution of 2°×2.5°, and 47 vertical layers.
235 The dry deposition module, which has been discussed above (W98), is driven by the monthly mean LAI retrieved from
236 Moderate Resolution Imaging Spectroradiometer (MODIS) (Myneni et al., 2002) and the 2001 version of Olson land cover
237 map (Olson et al., 2001). Both of the maps are binned from their native resolutions to 0.25°×0.25°.

238

239 We propose to estimate the sensitivity of surface O₃ concentrations to uncertainty/changes in v_d by the following equation:

240

$$\Delta O_3 = \beta \frac{\Delta v_d}{v_d}$$

241 where ΔO_3 is the response of monthly mean daytime surface O₃ to fractional change in v_d ($\Delta v_d/v_d$), and β accounts for the
242 sensitivity of surface O₃ concentration in a grid box to the perturbation in v_d within that grid box. To estimate β , we run two
243 simulations for the year 2013, one with default setting and another where we perturb v_d by +30%. Since not every gaseous
244 species deposit with the same functional relationships as O₃, we only adjust the v_d of O₃ to avoid perturbing the chemistry
245 resulting from the deposition of other chemically relevant species (e.g. PAN, HNO₃). Thus, this approach could represent a
246 conservative estimate of O₃ sensitivity to v_d if the impacts on other species result in additional effects on O₃. Nevertheless, we
247 use this sensitivity to estimate the potential impact of v_d simulation on surface O₃ concentration to a first order in subsequent
248 sections. This approach is based on the reasonably linear response of surface O₃ to v_d over comparable range of v_d change
249 (Wong et al., 2018). We limit our analysis to grid cells where the monthly average v_d is greater than 0.25 cm s⁻¹ in the baseline
250 simulation, since changes in surface O₃ elsewhere are expected to be attributed more to chemical transport rather than the local
251 perturbation of v_d (Wong et al., 2018).

252 3. Evaluation of Dry Deposition Parameterizations

253 We first compare our offline simulations of seasonal mean daytime average v_d that result from the four parameterizations in
254 the [Clim] and [Clim+LAI] scenarios with an observational database largely based on the evaluation presented in Silva and
255 Heald (2018). We use two unbiased and symmetrical statistical metrics, normalized mean bias factor (*NMBF*) and normalized
256 mean absolute error factor (*NMAEF*), to evaluate our parameterizations. Positive *NMBF* indicates that the parameterization
257 overestimates the observations by a factor of $1 + NMBF$ and the absolute gross error is *NMAEF* times the mean observation,
258 while negative *NMBF* implies that the parameterization underestimates the observations by a factor of $1 - NMBF$ and the



259 absolute gross error is *NMAEF* times the mean model prediction (Yu et al., 2006). We use the simulated subgrid land type-
260 specific predictions of v_d that correctly match the land type and the averaging window indicated by the observations. We
261 exclude instances where the observed land type does not have a match within the model grid box. While this leads to a reduction
262 of dataset size comparing to Silva and Heald (2018), this means that mismatched land-cover types can be ignored as a factor
263 in model bias.

264

265 Figure 1 shows the fractional coverage within each grid cell and the geographic locations of O_3 flux observation sites for each
266 major land type. Nearly all the observations are clustered in Europe and North America, except three sites in the tropical
267 rainforest and one site in tropical deciduous forest in Thailand. The resulting *NMBF* and *NMAEF* for five major land type
268 categories are shown in Table 2, and the list of sites and their descriptions are given in Table A3. In general, the numerical
269 ranges of both *NMBF* and *NMAEF* are similar to that of Silva and Heald (2018), and no single parameterization of the four
270 parameterizations outperforms the others across all five major land types. Here, we focus on describing how our
271 implementation of the dry deposition parameterizations produce consistent comparisons with earlier results.

272

273 As summarized in Table 2, each parameterization shows distinct biases over specific land types (we subsequently refer to
274 this as the “land-type specific bias” unique to each parameterization). Comparing the two multiplicative parameterizations
275 (W98 and Z03), we find that W98 performs satisfactorily over deciduous forests and tropical rainforests, while strongly
276 underestimating daytime v_d over coniferous forests. In contrast, Z03 performs better in coniferous forests but worse in
277 tropical rainforests and deciduous forests. The severe underestimation of daytime v_d by Z03 over tropical rainforests has
278 previously been attributed to persistent canopy wetness, and hence stomatal blocking imposed by the parameterization
279 (Centoni, 2017). The simple linear *VPD* response function in Z03 may overestimate the sensitivity of g_s to *VPD* under the
280 high temperature in tropical rainforest. We also note that even for the same location, v_d can vary significantly between
281 seasons (Rummel et al., 2007) and management practices (Fowler et al., 2011), which models may fail to capture due to
282 limited representations of land cover. Given the small sample size ($N = 5$), diverse environments, and large anthropogenic
283 intervention in the tropics, the disparity in performance metrics may not fully reflect the relative model performance.
284 Baseline cuticular resistances in Z03 under dry and wet canopy are 1.5 and 2 times that of coniferous forests, respectively
285 (Zhang et al., 2003), such that the enhancement of cuticular uptake by wetness may not compensate the reduced g_s over
286 tropical rainforests, and, to a lesser extent, deciduous forests. The higher cuticular uptake may explain the better performance
287 of Z03 over W98 over coniferous forests, where strong non-stomatal (though not necessarily cuticular) ozone sinks are often
288 observed (e.g. Gerosa et al., 2005; Wolfe et al., 2011).

289

290 Over grasslands, W98 has higher positive biases, while Z03 has higher absolute errors. This is because for datasets at high
291 latitudes, the dominant grass PFT is arctic grass, which is mapped to “tundra” land type (Geddes et al., 2016). While tundra
292 is parameterized similarly to grasslands in W98, this is not the case in Z03. Combined with the general high biases at other



293 sites for these parameterizations, the large low biases for “tundra” sites in Z03 lower the overall high biases but leads to
294 higher absolute errors.

295

296 Over croplands, the positive biases and absolute errors are relatively large for both W98 and Z03 (with Z03 performing
297 worse in general than W98). This may be attributed to the lack of response to *VPD* over all crop and grass land types in Z03.
298 The functional and physiological diversity with the “crop” land type also contributes to the general difficulty in simulating v_d
299 over cropland. Even though Z03 has individual parameterizations for 4 specific crop types (rice, sugar, maize and cotton),
300 this advantage is difficult to fully leverage as most global land cover data sets do not resolve croplands into such detail.

301

302 Substituting the native g_s in W98 and Z03 by that simulated by Ball-Berry model (the W98_BB and Z03_BB runs)
303 generally, though not universally, leads to improvement in model performance against the observations. W98_BB has
304 considerably smaller biases and absolute errors than W98 over grassland. While having little effect on the absolute error,
305 W98_BB improves the biases over coniferous forest and cropland compared to W98, but worsens the biases over rainforests
306 and deciduous forests. In contrast, Z03_BB is able to improve the model-observation agreement over all 5 land types when
307 compared to Z03. This finding echoes that from Wu et al. (2011), who explicitly show the advantage of replacing the g_s of
308 Wesely (1989) with the Ball-Berry model in simulating v_d over a forest site, and in addition shows the potential of Ball-Berry
309 model in improving spatial distribution of mean v_d .

310

311 The minimal impact that results from using LAI that matches the time of observation is not unexpected, since the
312 meteorological and land cover information from a $2^\circ \times 2.5^\circ$ grid cell may not be representative of the typical footprint of a site
313 measurement (on the order of 10^{-3} to 10^1 km², e.g. Chen et al., 2009, 2012). This problem has also been highlighted in
314 previous evaluation efforts in global-scale CTMs (Hardacre et al., 2015; Silva and Heald, 2018). Furthermore, the sample
315 sizes for all land types are small ($N \leq 16$) and the evaluation may be further compromised by inherent sampling biases.

316

317 In addition to the evaluation against field observation, we find good correlation ($R^2 = 0.94$) between the annual mean v_d from
318 GEOS-Chem at 2013 and the 30-year mean v_d of W98 run with static LAI. Overall, our evaluation shows that the quality of
319 our offline simulation of dry deposition across the four parameterizations in this work is largely consistent with previous
320 global modelling evaluation efforts.

321 **4. Impact of Dry Deposition Parameterization Choice on Long-Term Averages**

322 Here we summarize the impact that the different dry deposition parameterizations may have on simulations of the spatial
323 distribution of v_d and on the inferred surface O₃ concentrations. We begin by comparing the simulated long-term mean v_d
324 across parameterizations, then use a chemical transport model sensitivity experiment to estimate the O₃ impacts.



325
326 Figure 2 shows the 30-year July daytime average v_d simulated by W98 over vegetated surfaces (defined as the grid cells with
327 >50% plant cover), and Figure 3 shows the difference between the W98 and the W98_BB, Z03, Z03_BB predictions
328 respectively. We first focus on results from July because of the coincidence of high surface O_3 level, biospheric activity and
329 v_d in the Northern Hemisphere (NH), and will subsequently discuss the result for December, when such condition holds for
330 the Southern Hemisphere (SH). W89 simulates the highest July mean daytime v_d in Amazonia (1.2 to 1.4 cm s^{-1}), followed by
331 other major tropical rainforests, and temperate forests in northeastern US. July mean daytime v_d in other temperate regions in
332 North America and Eurasia typically range from 0.5 to 0.8 cm s^{-1} , while in South American and African savannah, and most
333 parts of China, daytime v_d is around 0.4 to 0.6 cm s^{-1} . In India, Australia, western US, and polar tundra Mediterranean region,
334 July mean daytime v_d is low (0.2-0.5 cm s^{-1}) which could be due to either the high temperature or the sparsity of vegetation (or
335 a combination of both).

336
337 The other three parameterizations (W98_BB, Z03, Z03_BB) simulate substantially different spatial distributions of daytime
338 v_d . In North America, we find W98_BB, Z03 and Z03_BB produce lower v_d (by -0.1 to -0.4 cm s^{-1}) compared to W98 in
339 deciduous forest-dominated northeastern US and slightly higher v_d in boreal forest-dominated regions of Canada. Z03 and
340 Z03_BB produce noticeably lower v_d (by up to -0.2 cm s^{-1}) in arctic tundra and grasslands in western US. In southeastern US,
341 W98_BB and Z03_BB simulate a slightly higher v_d (by up to +0.1 cm s^{-1}), while Z03 suggests a slightly lower v_d (by up to -
342 0.1 cm s^{-1}). W98_BB simulates a lower (-0.1 to -0.4 cm s^{-1}) v_d in tropical rainforests, with larger reductions concentrated in
343 southern Amazonia, where July is within the dry season, while the northern Amazonia is not (Malhi et al., 2008). Z03 and
344 Z03_BB simulate much smaller (-0.4 to -0.6 cm s^{-1}) v_d in all tropical rainforests.

345
346 Over the midlatitudes in Eurasia, Australia and South America except Amazonia, W98_BB, Z03 and Z03_BB generally
347 simulate a lower daytime v_d by up to 0.25 cm s^{-1} , possibly due to the dominance of grasslands and deciduous forests, where
348 W98 tends to be more high-biased than other parameterizations when compared to the observations of v_d . In southern African
349 savannah, W98_BB and Z03_BB suggest a much lower daytime v_d (by -0.1 to -0.4 cm s^{-1}) because of explicit consideration of
350 soil moisture limitation to A_n and g_s . Z03_BB simulates a particularly high daytime v_d over the high-latitude coniferous forests
351 (+0.1 to +0.3 cm s^{-1}). W98_BB and Z03_BB produce higher daytime daytime v_d (up to +0.15 cm s^{-1}) in India and South China
352 due to temperature acclimation (Kattge and Knorr, 2007), which allows more stomatal opening under the high temperature
353 that would largely shut down the stomatal deposition in W98 and Z03, as long as the soil does not desiccate. This is guaranteed
354 by the rainfall from summer monsoon in both regions. Low v_d is simulated by Z03 and Z03_BB in the grasslands near Tibetan
355 plateau because the grasslands are mainly mapped to tundra land type, which typically has low v_d as discussed in section 3.

356
357 Our results suggest that the global distribution of simulated mean v_d depends substantially on the choice of dry deposition
358 parameterization, driven primarily by the response to hydroclimate and land type-specific parameters, which could impact the



359 spatial distribution of surface ozone predicted by chemical transport models. To estimate the impact on surface ozone of an
360 individual parameterization “*i*” compared to the W98 predictions (which we use as a baseline), we apply the following
361 equation:

362
$$\Delta O_{3,i} \approx \beta \frac{\overline{v_{d,i}}}{\overline{v_{d,W98}}} \quad (3)$$

363 where $\Delta O_{3,i}$ is the estimated impact on simulated O_3 concentrations in a grid box, $\Delta \overline{v_{d,i}}$ is the difference between
364 parameterization *i* and W98 simulated mean daytime v_d in that grid box, $\overline{v_{d,W98}}$ is W98 output mean daytime v_d for that grid
365 box, and β is the sensitivity of surface ozone to v_d calculated by the method outlined in Section 2.3

366

367 Figure 4 shows the resulting estimates of ΔO_3 globally. We find ΔO_3 is the largest in tropical rainforests for all the
368 parameterizations (up to 5 to 8 ppbv), which agrees with the result from Centoni (2017). Other hotspots of substantial
369 differences are boreal coniferous forests, eastern US, continental Europe, Eurasian steppe and the grassland in southwestern
370 China, where ΔO_3 is either relatively large or the signs disagree among parameterizations. In India, Indochina and South China,
371 ΔO_3 is relatively small but still reaches up to up to -2 ppbv. We find that ΔO_3 is not negligible (1-4 ppbv) in many regions with
372 relatively high population density, which suggests that the choice of dry deposition parameterization can be relevant to the
373 uncertainty in the study of air quality and its implication on public health. We note that we have not estimated ΔO_3 for some
374 regions with low GEOS-Chem-predicted v_d ($< 0.25 \text{ cm s}^{-1}$, as described in section 2.3), but where the disagreement in v_d
375 between parameterizations can be large (e.g., southern African savannah, see Figure 3). Given this limitation, the impacts on
376 O_3 we have summarized may therefore be spatially conservative.

377

378 To explore the importance of seasonality in predictions of v_d and their subsequent impact, we repeat the above analyses for
379 December. Figure 5 shows the 1982-2011 mean December daytime v_d predicted by W98, while Figure 6 shows the difference
380 between W98 and the Z03, W98_BB, Z03_BB respectively. High latitudes in the NH are excluded due to the small number of
381 daytime hours. Z03 and Z03_BB simulate substantially lower in daytime v_d at NH midlatitudes because Z03 and Z03_BB
382 allow partial snow cover but W98 and W98_BB only allow total or no snow cover. At midlatitudes, the snow cover is not high
383 enough to trigger the threshold of converting vegetated to snow covered ground in W98 and W98_BB, resulting in lower
384 surface resistance, and hence higher daytime v_d comparing to Z03 and Z03_BB. In Amazonia, the hotspot of difference in
385 daytime v_d shifts from the south to the north, which is in the dry season (Malhi et al., 2008). These results for December,
386 together with our findings from July, suggest that the discrepancy in simulated daytime v_d between W98 and other
387 parameterizations is due to the explicit response to hydroclimate in the former compared to the latter. Given that field
388 observations indicate a large reduction of v_d in dry season in Amazonia (Rummel et al., 2007), the lack of dependence of
389 hydroclimate can be a drawback of W98 in simulating v_d in Amazonia.

390



391 Figure 7 shows the resulting estimates of ΔO_3 globally for December using Equation 3. In all major rainforests, ΔO_3 is smaller
392 in December due to generally lower sensitivity compared to July. A surprising hotspot of both daytime Δv_d and ΔO_3 is the
393 rainforest/tropical deciduous forest in Myanmar and its eastern bordering region, which also has distinct wet and dry season.
394 The proximity of December to the dry season, which starts at January (e.g. Matsuda et al., 2005), indicates that the consistent
395 Δv_d between W98 and other parameterizations is driven by hydroclimate as in Amazonia. Comparison with field measurements
396 (Matsuda et al., 2005) suggests that the W98_BB and Z03_BB capture daytime v_d better than W98, while Z03 may
397 overemphasize the effect of such dryness. The above reasoning also explains some of the Δv_d in India and south China across
398 the three parameterizations. These findings identify hydroclimate as a key driver of process uncertainty of v_d , and therefore its
399 impact on the spatial distribution of surface ozone concentrations, independent of land type-based biases.

400

401 Overall, these results demonstrate that the discrepancy in the spatial distribution of simulated mean daytime v_d resulting from
402 choice of dry deposition parameterization can have an important impact on the global distribution of surface O_3 predicted by
403 chemical transport models. We find that the response to hydroclimate by individual parametrization not only affects the mean,
404 but also the seasonality, of predicted surface O_3 , which is complementary to the findings of Kavassalis and Murphy (2017)
405 that mainly focus on how shorter-term hydrometeorological variability may modulate surface O_3 through dry deposition.

406

407 5. Impact of Dry Deposition Parameterization Choice on Trends and Interannual Variability

408 Here we explore the impact that different dry deposition parameterizations may have on predictions of IAV and trends in v_d
409 and on the inferred surface O_3 concentrations. We use Theil-Sen method (Sen, 1968) to estimate trends in July daytime v_d (and
410 any underlying meteorological variables), and use p-value < 0.05 to estimate significance.

411

412 Figure 8 shows the trend in July mean daytime v_d from 1982-2011 predicted by each of the parameterizations and scenarios
413 ([Clim], [Clim + LAI], and [Clim + LAI + CO₂]). Figure 9 shows the potential impact of these trends in v_d on July daytime
414 surface ozone, which we estimate to a first order using the following equation:

$$415 \Delta O_{30y,i} \approx \beta \times (\text{Annual \% change in } v_{d,i}) \times 30 \text{ years} \quad (4)$$

416 where $\Delta O_{30y,i}$ is the absolute change in ozone inferred to a first order as a result of the trend v_d for parameterization i over the
417 30-years (1982-2011).

418

419 In [Clim] simulations (where LAI is held constant), the trend of July daytime v_d is either small or non-significant over the vast
420 majority of the NH. An exception is observed in the region of Mongolia, where significant increasing trend in T (warming)
421 and decreasing trend in RH (drying) detected in the MERRA-2 surface meteorological field in July daytime results in
422 significant decreasing trends using the Z03, W98_BB and Z03_BB parameterizations. This trend is not present in the W98



423 parameterization as this formulation does not respond to the long-term drying. We find some decreasing trends in v_d across
424 parts of central Europe and the Mediterranean to varying degrees across the parameterizations. In the SH, we find consistent
425 decreasing trends across all four parameterizations in southern Amazonia and southern African savannah due to warming and
426 drying, which we estimate could produce a concomitant increase in July mean surface ozone of between 1 to 3 ppbv (Figure
427 9).

428

429 In [Clim+LAI] scenario, all four parameterizations simulate a significant increasing trend of v_d over high latitudes, which is
430 consistent with the observed greening trend over the region (Zhu et al., 2016). We estimate this could produce a concomitant
431 increase in July mean surface ozone of between 1 to 3 ppbv. The parameterizations generally agree in terms of the spatial
432 distribution of these trends in O_3 . Exceptions include a steeper decreasing trend in most of Siberia predicted by W98, while
433 the trend is more confined in the eastern and western Siberia in the other three parameterizations. Including the effect of CO_2 -
434 induced stomatal closure ([Clim+LAI+ CO_2] runs) partially offset the increase of v_d in high latitudes, but does not lead to large
435 changes in both the magnitudes and spatial patterns of v_d trend. We find negligible trends in daytime v_d for December in all
436 cases. These results show that across all dry deposition model parameterizations, LAI and climate, more than increasing CO_2 ,
437 can potentially drive significant long-term changes in v_d and should not be neglected when analyzing the long-term change in
438 air quality over 1982-2011. We note that the importance of the CO_2 effect could grow in the coming decades, since the
439 sensitivity of stomatal conductance to atmospheric CO_2 may increase (Franks et al., 2013).

440

441 We go on to explore the impact of parameterization choice in calculations of IAV in v_d . Figure 10 shows the coefficient of
442 variation of linearly detrended July daytime v_d (CV_{v_d}). Figure 11 shows the potential impact this has on IAV in surface ozone,
443 which we estimate to a first order by the following equation:

444
$$\sigma_{O_3,i} \approx \beta \times CV_{v_d,i} \quad (5)$$

445 where $\sigma_{O_3,i}$ is the estimated interannual standard deviation in surface ozone resulting from IAV in v_d given predicted by dry
446 deposition parameterization i . In both cases, we show only the [Clim] and [Clim+LAI] runs, since IAV in CO_2 has negligible
447 impact on interannual variability in v_d .

448

449 Using the W98 parameterization, IAV in predicted v_d and O_3 is considerably smaller in the [Clim] run than that for the [Clim
450 + LAI] run, since both the stomatal and non-stomatal conductance in W98 are strong functions of LAI rather than
451 meteorological conditions. This implies that long-term simulations with W98 and constant LAI can potentially underestimate
452 the IAV of v_d and surface ozone. In contrast, IAV in v_d calculated by the Z03 parameterization is nearly the same for the [Clim]
453 and [Clim+LAI] runs. In Z03, g_s is also directly influenced by VPD in addition to temperature and radiation, and non-stomatal
454 conductance in Z03 is much more dependent on meteorology than W98, leading to high sensitivity to climate. Though the
455 Ball-Berry model also responds to meteorological conditions, it considers relatively complicated A_n - g_s regulation and includes
456 temperature acclimation, which could dampen its sensitivity to meteorological variability compared to the direct functional



457 dependence on meteorology in the Z03 multiplicative algorithm. Thus, the climate sensitivity of W98_BB and Z03_BB is in
458 between Z03 and W98, as is indicated by more moderate difference between $\sigma_{O_3,i}$ from [Clim] and [Clim+LAI] runs in Figure
459 11.

460

461 For regional patterns of CV_{vd} and σ_{O_3} , we focus on the [Clim+LAI] runs (Fig. 10e to 10h and Fig. 11e to 11h) as it allows for
462 a comparison of all 4 parameterizations and contain all the important factors of controlling v_d . In North America, we estimate
463 modest IAV in v_d across all 4 parameterizations ($CV_{vd} < 15\%$) in most places. We find this results in relatively low σ_{O_3} in
464 northeastern US, and larger σ_{O_3} in central and southeast US (in the range of 0.3 to 2 ppbv). These results are of a similar
465 magnitude to the standard deviation of summer mean background ozone suggested by Fiore et al. (2014) over similar time
466 period, confirming that IAV of dry deposition can be a potentially important component of the natural IAV of surface ozone
467 in summer over North America.

468

469 All parameterizations produce larger CV_{vd} (and therefore larger σ_{O_3}) in southern Amazonia compared to northern and central
470 Amazonia, but we find substantial discrepancies across parameterizations. The estimated impact on IAV in O_3 (σ_{O_3}) in southern
471 Amazonia ranges from less than 1 ppbv predicted by the W98 and W98_BB parameterizations, to exceeding 1.5 - 2.5 ppbv
472 predicted by the Z03 parameterization. IAV is also relatively large in central Africa. We find that the parameterizations which
473 include a Ball-Berry formulation (W98_BB and Z03_BB) estimate higher IAV in this region (with σ_{O_3} varying between 1 to
474 4 ppbv), compared to the W98 and Z03 parameterizations (σ_{O_3} up to 2ppbv). We also note that the Ball-Berry formulations
475 show more spatial discontinuities compared to W98 and Z03. In our implementation of the Ball-Berry model, impact of soil
476 moisture on g_s is parameterized as a function of root-zone soil matric potential, which makes g_s very sensitive to variation in
477 soil wetness when the its climatology is near the point that triggers limitation on A_n and g_s . Given the large uncertainty in soil
478 data (Folberth et al., 2016), such sensitivity could be potentially artificial, which should be taken into consideration when
479 implementing Ball-Berry parameterizations in large-scale models despite their relatively good performance in site-level
480 evaluation.

481

482 Across Europe, the magnitude of IAV predicted by all four parameterizations show relatively good spatial consistency.
483 Simulated CV_{vd} is relatively low in western and northern Europe (<10%), which we estimate translates to less than 1 ppbv of
484 σ_{O_3} . We find larger CV_{vd} (and therefore large σ_{O_3}) over parts of southern Russia and Siberia (σ_{O_3} up to 2.5 ppbv) from all
485 parameterizations except W98. The local geographic distribution of CV_{vd} and σ_{O_3} also significantly differs among the
486 parameterizations. Z03 and Z03_BB simulate larger CV_{vd} in eastern Siberia than W98_BB, while W98 BB and Z03_BB predict
487 larger CV_{vd} over the southern Russian steppe than Z03. Finally, all four parameterizations estimate relatively low CV_{vd} and σ_{O_3}
488 in India, China and Southeast Asia.

489



490 We compare the simulated IAV of v_d from all four deposition parameterizations with those recorded by publicly available
491 long-term observations. The IAV predicted by all four parameterizations at Harvard Forest is between 3% to 7.9%, which is 2
492 to 6 times lower than that presented in the observations (19%) by Clifton et al. (2017). We find similar underestimates by all
493 four parameterizations compared to the long-term observation from Hyytiälä (Junninen et al., 2009; Keronen et al., 2003;
494 <https://avaa.tdata.fi/web/smart/smear/download>), where observed CV_{v_d} (11%) is significantly higher than that predicted by the
495 deposition parameterizations (3.5% - 7.1%). In Blodgett Forest, where O_3 uptake is more controlled by gas-phase reactions
496 (Fares et al., 2010; Wolfe et al., 2011), we find that the models underestimate the observed annual CV_{v_d} more seriously (~1%
497 - 3% compared to 12% in the observations). This suggests that the IAV of v_d may be underestimated across all deposition
498 parameterizations we investigated (and routinely used in simulations of chemical transport). Clifton et al. (2017) attribute this
499 to the IAV in non-stomatal deposition, while acknowledging the obscurity of the mechanisms driving such variability, implying
500 the difficulty in reproducing the observed IAV by existing parameterizations. The scarcity of long-term ozone flux
501 measurements (Fares et al., 2010, 2017; Munger et al., 1996; Rannik et al., 2012) limits our ability to benchmark the IAV in
502 our model simulations with observational datasets.

503

504 In summary, when both the variability in LAI and climate are considered, the IAV in simulated v_d translates to IAV in surface
505 O_3 of 0.5 - 2 ppbv in July for most region. Such variability is predicted to be particularly strong in southern Amazonian and
506 central African rainforest, where the predicted IAV in July surface O_3 due to dry deposition can be as high as 4 ppbv. This
507 suggests that IAV of v_d can be an important part of the natural variability of surface O_3 . The estimated magnitude of IAV is
508 also dependent of the choice of v_d parameterization, which highlights the importance of v_d parameterization choice on
509 modelling IAV of surface O_3 .

510 **6 Discussion and Conclusion**

511 We present the results of multidecadal global modelling of ozone dry deposition using four different ozone deposition
512 parameterizations that are representative of the major types of approaches of gaseous dry deposition modelling used in global
513 chemical transport models. The parameterizations are driven by the same assimilated meteorology and satellite-derived LAI,
514 which minimizes the uncertainty of model input across parameterization and simplifies interpretation of inter-model
515 differences. The output is evaluated against field observations and shows satisfactory performance. One of our main goals was
516 to investigate the impact of dry deposition parameterization choice on long-term averages, trends, and IAV in v_d over a
517 multidecadal timescale, and estimate the potential concomitant impact on surface ozone concentrations to a first order using a
518 sensitivity simulation approach driven by the GEOS-Chem chemical transport model.

519

520 We find that the performance of the four dry deposition parameterizations against field observations varies considerably over
521 land types, and these results are consistent with other evaluations, reflecting the potential issue that dry deposition



522 parameterizations can often be overfit to a particular set of available observations, requiring caution in their application at
523 global scales. We also find that using more ecophysiological realistic output g_s predicted by the Ball-Berry model can
524 generally improve model performance, but at the cost of high sensitivity to relatively unreliable soil data. However, the number
525 of available datasets of ozone dry deposition observation are still small and concentrated in North America and Europe. We
526 know of only one multi-season direct observational record in Asia and none in Africa, where air quality can be an important
527 issue. To better constraint regional dry deposition, effort must be made in making new observations of gaseous dry deposition
528 (Fares et al., 2017) especially in the under-sampled regions. We also find that many existing ozone flux measurements are not
529 usable for our evaluation purposes, since only F_{O_3} is reported in detail instead of v_d . Evaluation and development of ozone dry
530 deposition parameterizations would be greatly benefited if result of ozone flux measurements is reported in both F_{O_3} and v_d ,
531 or even have publically available ozone flux and other related micrometeorological variables, which allows both direct
532 evaluation of v_d and solves the mismatch between coarse model grids and the site (e.g. Wu et al., 2011, 2018).

533

534 We find substantial disagreement in the spatial distribution between the mean daytime v_d predicted by the different
535 parameterizations we tested. We find that these discrepancies are in general a function of both location and season. In NH
536 summer, v_d simulated by the 4 parameterizations are considerably different in many vegetation-dominated regions over the
537 world. We estimate that this could lead to around 2 to 5 ppbv in uncertainty of surface ozone concentration simulations over
538 a vast majority land in the NH. In tropical rainforests, where leaf wetness is prevalent and the dry-wet season dynamics can
539 have large impact on v_d (Rummel et al., 2007), we estimate the uncertainty due to dry deposition model choice could even
540 lead to an uncertainty in surface ozone of up to 8 ppbv. We also find noticeable impacts in parameterization choice during
541 SH summer, but we note that due to the unreliability of β at low v_d , we have not assessed its impact on surface ozone in
542 many high-latitude regions of the NH. In general, we find hydroclimate to be an important driver of the uncertainty. This
543 demonstrates the potential impact of parameterization choice (or, process uncertainty) of v_d is neither spatiotemporally
544 uniform nor negligible in most vegetated regions over the world. More multi-seasonal observations are especially needed
545 over seasonally dry ecosystems where the role of hydroclimate in deposition parameterizations need to be evaluated.
546 Recently, standard micrometeorological measurements have been used to derive g_s and stomatal deposition of O_3 over North
547 America and Europe (Ducker et al., 2018), highlighting the potential of using global networks of micrometeorological
548 observation (e.g. FLUXNET (Baldocchi et al., 2001)) to benchmark and calibrate g_s of dry deposition parameterizations,
549 which could at least increase the spatiotemporal representativeness, if not the absolute accuracy, of dry deposition
550 parameterizations.

551

552 Over the majority of vegetated regions in the NH, we estimate the IAV of mean daytime v_d is generally on the order of 5 to
553 15% and may contribute between 0.5 to 2 ppbv of IAV in July surface O_3 over the thirty-year period considered here, with
554 each parameterization simulating different geographic distribution of where IAV is highest. The predicted IAV from all four
555 models is smaller than what long-term observations suggest, but is still comparable to the long-term variability of background



556 ozone over similar timescales in U.S. summer (Brown-Steiner et al., 2018; Fiore et al., 2014). This would seem to confirm that
557 v_d may be a substantial contributor to natural IAV of O_3 in summer, at least in U.S. In the southern Hemisphere, the IAV
558 mainly concentrates in drier part of tropical rainforests. The Ball-Berry parameterizations simulate large and spatially
559 discontinuous CV_{v_d} and σ_{O_3} due to their sensitivity to soil wetness. Globally, we find that IAV of v_d in W98 is mostly driven
560 by LAI, while in other parameterizations climate generally plays a more important role. We therefore emphasize that temporal
561 matching of LAI is important for consistency when W98 is used in long-term simulations. The scarcity of long-term ozone
562 deposition measurement poses significant difficulty in evaluating the model predictions over interannual (and in particular
563 multidecadal) timescales. This information is helpful in designing and identifying sources of error in model experiments that
564 involve variability of v_d .

565

566 We are also able to detect statistically significant trends in July daytime v_d over several regions. The magnitudes of trend are
567 up to 1% per year and both climate and LAI contribute to the trend. All four deposition parameterizations identify three main
568 hotspots of decreasing July daytime v_d (southern Amazonia, southern African savannah, Mongolia), which we link mainly to
569 increasing surface air temperature and decreasing relative humidity. Meanwhile, extensive areas at high latitudes experience
570 LAI-driven increasing July daytime v_d , consistent with the greening trend in the region (Zhu et al., 2016). We don't find a
571 strong influence of CO_2 -induced stomatal closure in the trend over this time period. Over the 30-years we estimate the trend
572 in July daytime v_d could translate approximately to 1 to 3 ppbv of ozone changes in the areas of impact, indicating the potential
573 effect of long-term changes in v_d on surface ozone. This estimate should be considered conservative, since we are unable to
574 reliably test the sensitivity of ozone to regions with low v_d with our approach.

575

576 While the approach we have presented here allows us to explore the role of dry deposition parameterization choice on
577 simulations of long-term means, trends, and IAV in ozone dry deposition velocity, there remain some limitations and
578 opportunities for development. First, we only used one LAI and assimilated meteorological product. The geographic
579 distribution of trend and IAV of v_d may vary considerably as the LAI and meteorological products used due to their inherent
580 uncertainty (e.g. Jiang et al., 2017). While we expect the qualitative conclusions about how LAI and climate controls the
581 modelled trend and IAV of v_d to be robust to the choice of data set, the magnitude and spatial variability could be affected.
582 Second, the estimated effects on surface O_3 are a first-order inference based on a linear approximation of the impact that v_d
583 has directly on O_3 . We have not applied our analysis to regions with low baseline GEOS-Chem v_d , where other components of
584 parameterization (e.g. definition and treatment of snow cover, difference in ground resistance) may have major impact on v_d
585 prediction (Silva and Heald, 2018), nor accounted for the role that v_d variability can have on other chemical species which
586 would have feedbacks on O_3 . Moreover, the sensitivity of surface ozone to dry deposition velocity may be dependent on the
587 choice of chemical transport model (here, the GEOS-Chem model has been used), and possibly the simulation year. Finally,
588 we have neglected the effect of land use and land cover change on global PFT composition at this stage, which can be another
589 source of variability for v_d . Nevertheless, the relatively high *NMAEF* of simulated v_d and the inherent uncertainty in input data



590 (land cover, soil property, assimilated meteorology and LAI) are considered as the major source of uncertainty in our
591 predictions of v_d .

592

593 The impact of dry deposition parameterization choice may be generalizable to other trace gases with deposition velocity
594 controlled by surface resistance, and for which stomatal resistance is an important control of surface resistance (e.g. NO₂). As
595 v_d has already been recognized as a major source of uncertainty in deriving global dry deposition flux of NO₂ and SO₂ (Nowlan
596 et al., 2014), systematic investigation on the variability and uncertainty of v_d for other relevant chemical species does not only
597 contribute to understanding the of gaseous dry deposition role on air quality, but also biogeochemical cycle. Particularly,
598 gaseous dry deposition has been shown to be a major component in nitrogen deposition (Geddes and Martin, 2017; Zhang et
599 al., 2012), highlighting the potential importance of understanding the role of v_d parameterization in modelling regional and
600 global nitrogen cycle.

601

602 Here we have built on the recent investigations of modelled global mean (Hardacre et al., 2015; Silva and Heald, 2018) and
603 observed long-term variability (Clifton et al., 2017) of O₃ v_d . We are able to demonstrate the substantial impact of v_d
604 parameterization on modelling the global mean and IAV of v_d , and their non-trivial potential impact on simulated seasonal
605 mean and IAV of surface ozone. We demonstrate that the parameterizations with explicit dependence on hydroclimatic
606 variables have higher sensitivity to climate variability than those without. Difficulties in evaluating predictions of v_d for many
607 regions of the world (e.g. most of Asia and Africa) persist due to the scarcity of measurement. This makes a strong case for
608 additional measurements (e.g. Kammer et al., 2019; Li et al., 2018; Stella et al., 2011a), empirical studies (e.g. Ducker et al.,
609 2018) and model-observation integrations (e.g. Silva et al., 2019) of ozone dry deposition at different timescales, which would
610 be greatly facilitated by an open data sharing infrastructure (e.g. Baldocchi et al., 2001; Junninen et al., 2009).

611 Code Availability

612 The source code and output of the dry deposition parameterizations can be obtained by contacting the corresponding author
613 (jgeddes@bu.edu).

614 Appendix

	W98	Z03	W98_BB	Z03_BB
R_a	$R_a = \frac{1}{\kappa u_*} \left[\ln\left(\frac{z}{z_0}\right) - \Psi\left(\frac{z}{L}\right) + \Psi\left(\frac{z_0}{L}\right) \right]$ <p>When $\zeta \geq 0$, $\Psi(\zeta) = -5\zeta$</p> <p>When $\zeta < 0$, $\Psi(\zeta) = 2 \ln\left(\frac{1+\sqrt{1-16\zeta}}{2}\right)$</p>			



R_b	$R_b = \frac{2}{\kappa u_*} \left(\frac{Sc}{Pr} \right)^{2/3}$			
R_s	$R_s = r_s(PAR, LAI) f_T \frac{D_{H_2O}}{D_{O_3}}$	$R_s = \frac{r_s(PAR, LAI)}{(1 - w_{st}) f_T f_{vpd} f_\psi} \frac{D_{H_2O}}{D_{O_3}}$	$g_s = g_0 + m \frac{A_n}{C_s} h_s$ $R_s = \frac{1}{g_s} \frac{D_{H_2O}}{D_{O_3}}$	$g_s = g_0 + m \frac{A_n}{C_s} h_s$ $R_s = \frac{1}{(1 - w_{st}) g_s} \frac{D_{H_2O}}{D_{O_3}}$
Cuticular Resistance (R_{cut})	$R_{cut} = \frac{R_{cut0}}{LAI}$	For dry surface, $R_{cut} = \frac{R_{cutd0}}{e^{0.03RH} LAI^{0.25} u_*}$ For wet surface, $R_{cut} = \frac{R_{cutw0}}{LAI^{0.5} u_*}$	Same as W98	Same as Z03
In-canopy aerodynamic resistance (R_{ac})	Prescribed	$R_{ac} = R_{ac0} \frac{LAI^{0.25}}{u_*}$		
Ground Resistance (R_g)	Prescribed			
Lower-canopy aerodynamic resistance (R_{alc})	$R_{alc} = 100 \left(1 + \frac{1000}{R + 10} \right)$	-		
Lower-canopy surface resistance (R_{cls})	Prescribed	-		

615 **Table A1:** Brief description of the four dry deposition parameterizations. κ = von Karman constant, u_* = friction velocity, z =
 616 reference height, z_0 = roughness length, L = Obukhov length, Sc = Schmidt's number, Pr = Prandtl number for air, LAI = leaf
 617 area index, PAR = photosynthetically active radiation, D_x = Diffusivity of species x in air, f_T = temperature (T) stress function,
 618 f_{vpd} = vapour pressure deficit (VPD) stress function, f_ψ = leaf water potential (ψ) stress function, w_{st} = stomatal blocking fraction,
 619 A_n = Net photosynthetic rate, g_0 = minimum stomatal conductance, m = Ball-Berry slope, C_s = CO_2 concentration on leaf
 620 surface, h_s = relative humidity on leaf surface, RH = relative humidity, h = canopy height, R = downward shortwave radiation
 621

CLM PFT	Z03 surface type
Needleleaf evergreen tree - temperate	Evergreen needleleaf trees
Needleleaf evergreen tree - boreal	
Needleleaf deciduous tree - boreal	Deciduous needleleaf trees



Broadleaf evergreen tree - tropical	Tropical broadleaf trees
Broadleaf deciduous tree - tropical	Deciduous broadleaf trees
Broadleaf deciduous tree - temperate	
Broadleaf deciduous tree - boreal	
Broadleaf evergreen shrub - temperate	Thorn shrubs
Broadleaf deciduous shrub - temperate	Deciduous shrubs
Broadleaf deciduous shrub - boreal	
C ₃ arctic grass	Tundra
C ₃ grass	Short grass
C ₄ grass	Corn*
C ₃ crop	Crops

622 **Table A2:** Mapping between CLM PFT and Z03 surface type.

623 *C₄ grasses are mapped to corn due to the similarity in photosynthetic pathway, and hence stomatal control

624

Land Type	Longitude	Latitude	Season	Mean daytime v_d (cm s ⁻¹)	Citation
Deciduous Forest	-80.9°	44.3°	Summer	0.92	Padro et al., 1991
			Winter	0.28	
	99.7°	18.3°	Spring	0.38	Matsuda et al., 2005
			Summer	0.65	
	-72.2°	42.7°	Summer	0.61	Munger et al., 1996
			Winter	0.28	
-78.8°	41.6°	Summer	0.83	Finkelstein et al., 2000	
-75.2°	43.6°	Summer	0.82		
Coniferous Forest	-3.4°	55.3°	Spring	0.58	Coe et al., 1995
	-79.1°	36.0°	Spring	0.79	Finkelstein et al., 2000
	-120.6°	38.9°	Spring	0.58	Kurpius et al., 2002
			Summer	0.59	
			Autumn	0.43	
			Winter	0.45	
	-0.7°	44.2°	Summer	0.48	Lamaud et al., 1994
	105.5°	40.0°	Summer	0.39	Turnipseed et al., 2009
	-66.7°	54.8°	Summer	0.26	Munger et al., 1996
11.1°	60.4°	Spring	0.31	Hole et al., 2004	



			Summer	0.48	
			Autumn	0.20	
			Winter	0.074	
	8.4°	56.3°	Spring	0.68	Mikkelsen et al., 2004
			Summer	0.80	
			Autumn	0.83	
Tropical Rainforest	117.9°	4.9°	Wet	0.5	Fowler et al., 2011 [#]
			Wet	1.0	
	-61.8°	-10.1°	Wet	1.1	Rummel et al., 2007
			Dry	0.5	
	-60.0°	3.0°	Wet	1.8	Song-Miao et al., 1990
Grass	-88.2°	40.0°	Summer	0.56	Droppo, 1985
	-3.2°	57.8°	Spring	0.59	Fowler et al., 2001
			Summer	0.56	
			Autumn	0.42	
	-119.8°	37.0°	Summer	0.15	Padro et al., 1994
	-8.6°	40.7°	Summer	0.22	Pio et al., 2000
			Winter	0.38	
	-104.8°	40.5°	Spring	0.22	Stocker et al., 1993
	10.5°	52.4°	Spring	0.44	Mészáros et al., 2009
-96.4°	39.5°	Summer	0.62	Gao and Wesely, 1995	
Crops	-2.8°	55.9°	Not applicable*	0.69	Coyle et al., 2009
	-88.4°	40.1°		0.53	Meyers et al., 1998
				0.12	
				0.85	
	-87.0°	36.7°		0.39	
	-86.0°	34.3°		0.40	
	-120.7°	36.8°		0.76	Padro et al., 1994
	8.0°	48.7°		0.41	Pilegaard et al., 1998
	2.0°	48.9°		0.60	Stella et al., 2011
	0.6°	44.4°		0.47	
1.4°	43.8°	0.37			

625 **Table A3:** Information of all the measurement sites included in model evaluation



626 *Crops are heavily influenced by management practices rather than natural seasonality. Thus, two data sets in the same location
627 generally represent before and after certain a crop phenology or human management event.

628 #The two measurements are taken at a rainforest and an oil palm plantation nearby.

629

630 **Author Contributions**

631 AYHW and JAG developed the ideas behind this study, formulated the methods, and designed the model experiments. AYHW
632 wrote the dry deposition code and ran the chemical transport model simulations. Data analysis was performed by AYHW, with
633 input and feedback from JAG. APKT provided the photosynthesis model code, and co-supervised the dry deposition code
634 development. SJS compiled the dry deposition observations used for evaluation. Manuscript preparation was performed by
635 AYHW, reviewed by JAG, and commented, edited, and approved by all authors.

636 **Acknowledgement**

637 This work was funded by an NSF CAREER grant (ATM-1750328) to project PI J.A. Geddes; and the Vice-Chancellor
638 Discretionary Fund (Project ID: 4930744) from The Chinese University of Hong Kong (CUHK) given to the Institute of
639 Environment, Energy and Sustainability. Funding support to SJS was provide by a National Science Foundation grant to C.L.
640 Heald (ATM-1564495). We also thank the Global Modelling and Assimilation Office (GMAO) at NASA Goddard Flight
641 Center for providing the MERRA-2 data, Ranga Myneni for GIMMS LAI3g product, Petri Keronen and Ivan Mammarella for
642 the flux measurements in Hyytiala, Silvano Fares and Allen Goldstein for the flux measurement in Blodgett Forest, and
643 Leiming Zhang and Zhiyong Wu for the source code of Z03.

644

645

646

647

648

649

650

651

652

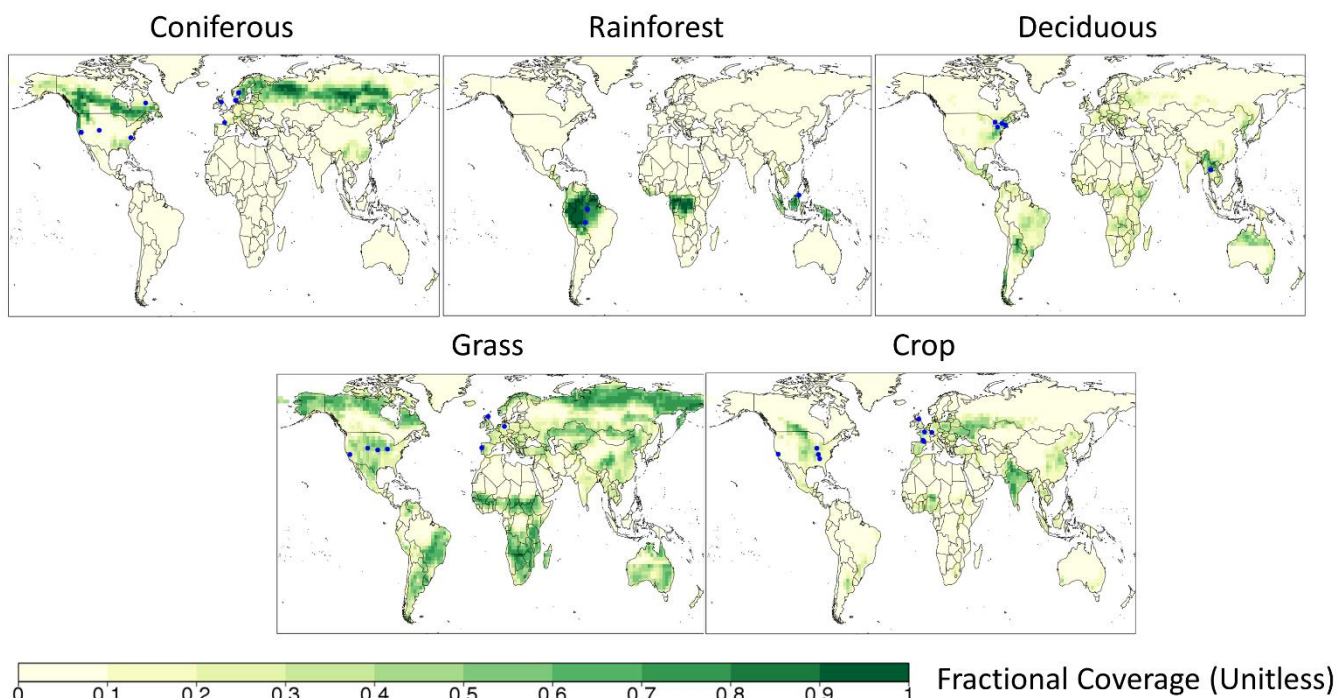
653

654

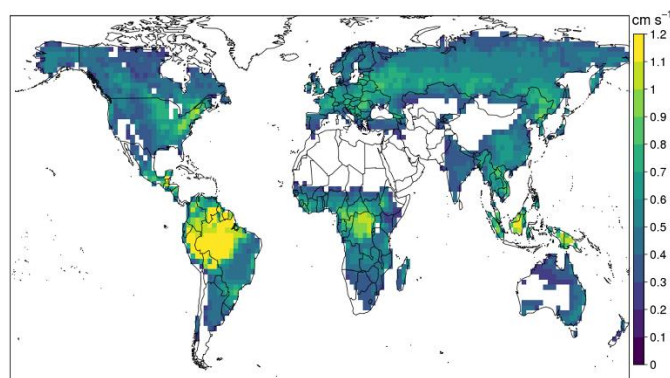
655



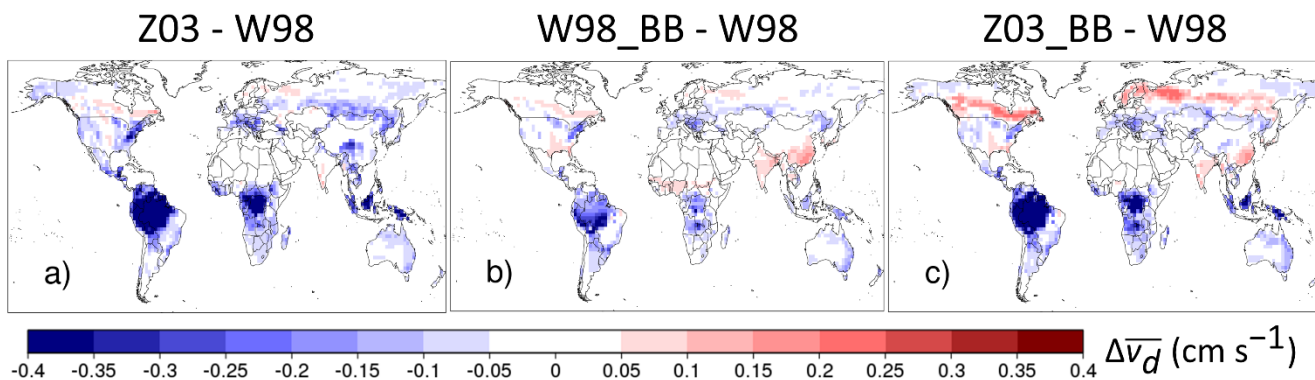
656
657
658



659
660 **Figure 1:** Fractional coverage of each major land type at each grid cell. Blue dots indicate the locations of the observational
661 sites.



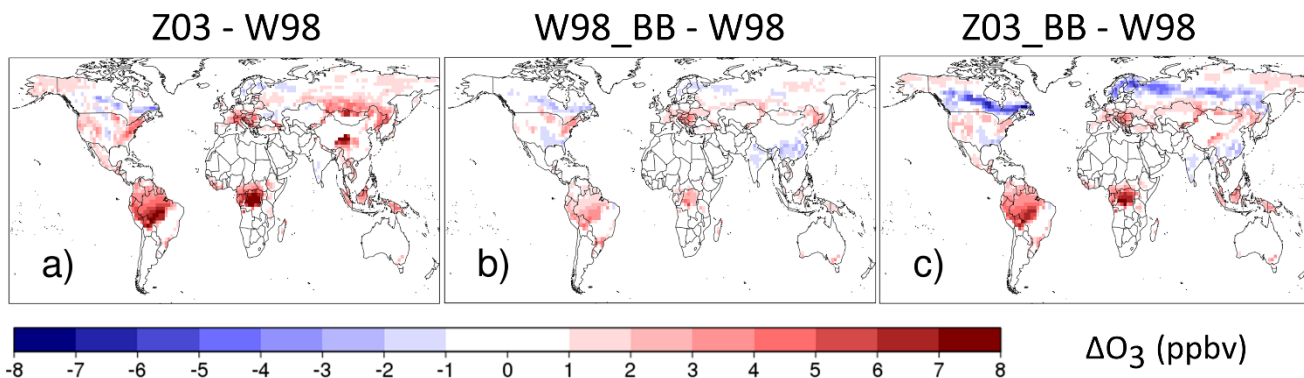
662
663 **Figure 2:** 1982-2011 July mean daytime v_u (solar elevation angle $> 20^\circ$) over vegetated land surface simulated by W98.
664



665

666 **Figure 3:** Differences of 1982-2011 July mean daytime v_d ($\Delta \bar{v}_d$) between three other parameterizations (Z03, W98_BB and
667 Z03_BB) and W98 over vegetated land surface.

668



669

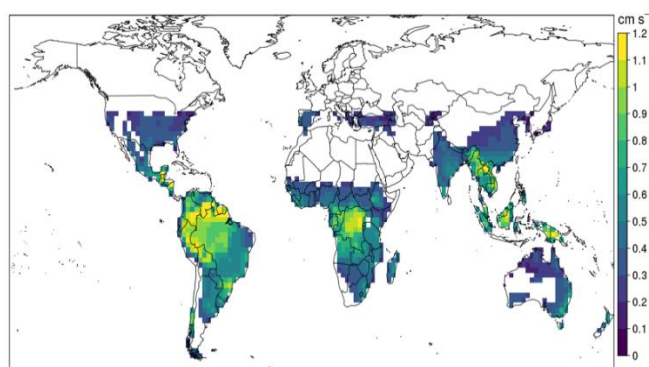
670 **Figure 4:** Estimated difference in July mean surface ozone (ΔO_3) due to the discrepancy of simulated July mean daytime v_d
671 among the parameterizations.

672

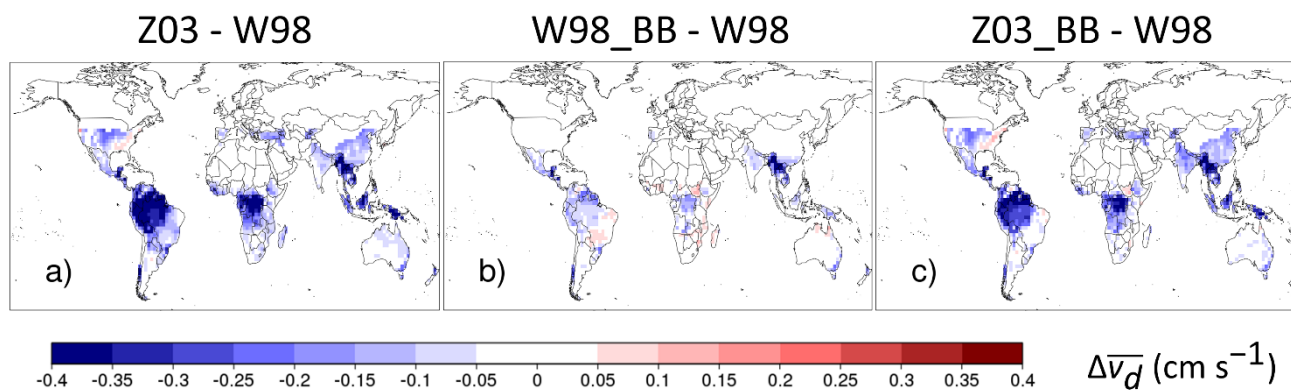
673

674

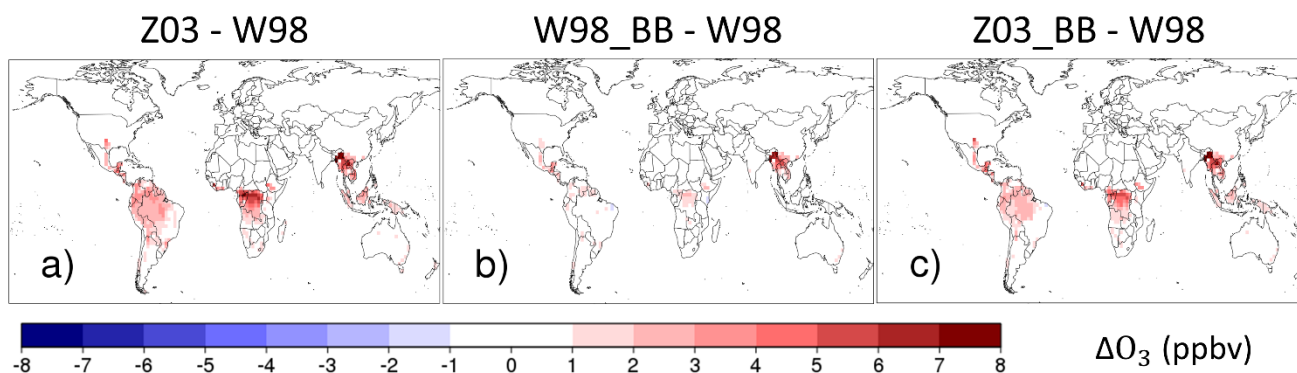
675



676
677 **Figure 5:** 1982-2011 December mean daytime v_d (solar elevation angle $> 20^\circ$) over vegetated land surface simulated by
678 W98. The data over high latitudes over Northern Hemisphere is invalid due to insufficient daytime hours over the month ($<$
679 100 hours month $^{-1}$)
680



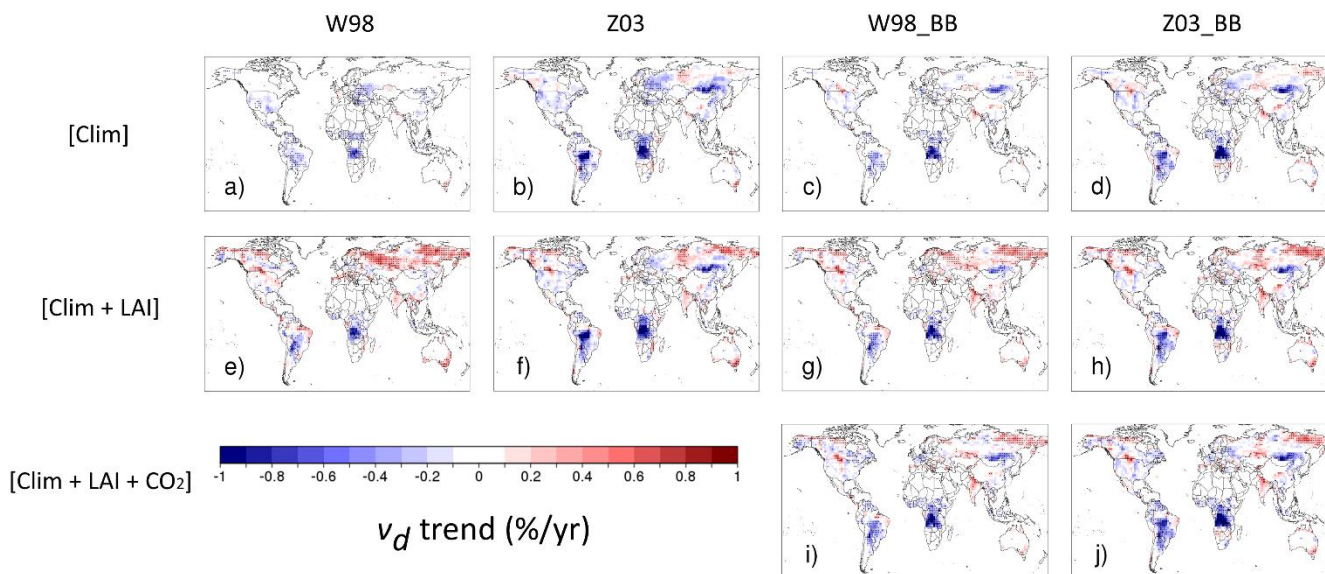
681
682 **Figure 6:** Differences of 1982-2011 December mean daytime v_d ($\Delta \bar{v}_d$) between three other parameterizations (Z03, W98_BB
683 and Z03_BB) and W98 over vegetated land surface.
684
685



686

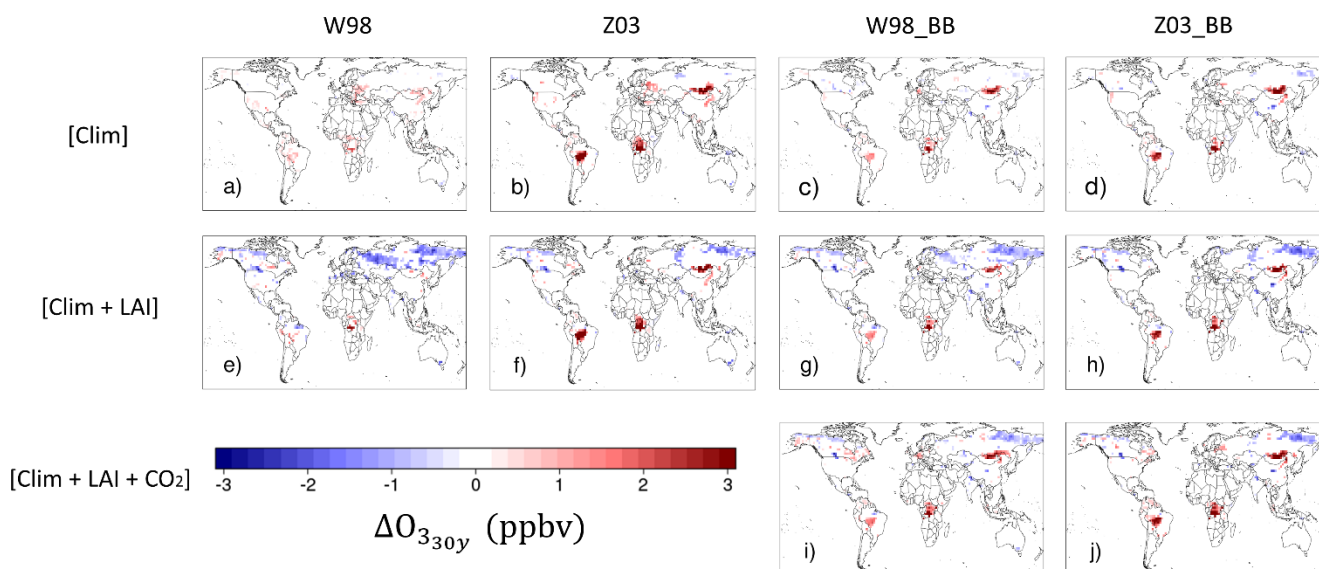
687 **Figure 7:** Estimated difference in December mean surface ozone (ΔO_3) due to the discrepancy of simulated December mean
 688 daytime v_d among the parameterizations.

689
 690

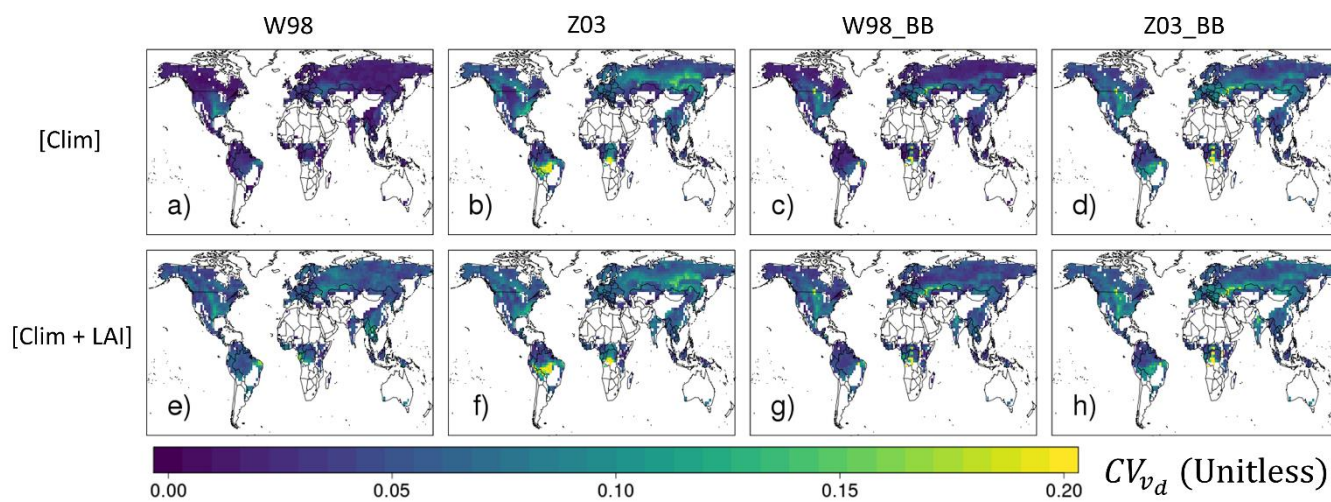


691

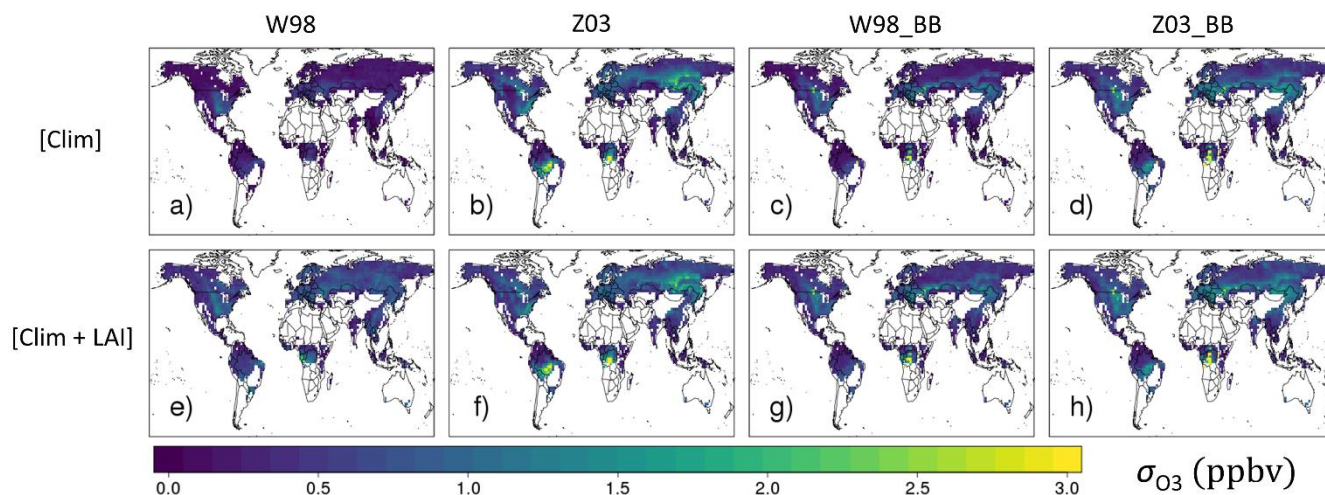
692 **Figure 8:** Trends of July mean daytime v_d during 1982-2011 over vegetated land surface. Black dots indicate statistically
 693 significant trends ($p < 0.05$)



694
 695 **Figure 9:** Estimated impact of trends of July mean daytime v_d on July mean surface ozone during ($\Delta O_{3\ 30y}$) 1982-2011 over
 696 vegetated land surface. Only grid points with statistically significant trends ($p < 0.05$) in July mean daytime v_d are
 697 considered.
 698



699
 700 **Figure 10:** Interannual coefficient of variation of linearly detrended July mean daytime v_d (CV_{v_d}) during 1982-2011 over
 701 vegetated land surface.



702

703 **Figure 11:** Estimated contribution of IAV in July mean daytime v_d to IAV of July mean surface ozone (σ_{O_3}) during 1982-
 704 2011 over vegetated land surface.

705

706

707

708

709

710

711

712

v_d simulation	Meteorology	LAI	Atmospheric CO ₂ concentration
[Clim]	MERRA-2 meteorology	LAI3g monthly climatology	390 ppm
[Clim+LAI]		LAI3g monthly time series	
[Clim+LAI+CO ₂]			Manoa Loa time series

713 **Table 1:** List of v_d simulations with input data

714

Land types	Metrics	Static LAI				Dynamic LAI			
		W98	Z03	W89-BB	Z03_BB	W98	Z03	W89-BB	Z03_BB
Dec (N=8)	<i>NMBF</i>	0.134	-0.367	-0.287	-0.142	0.119	-0.376	-0.299	-0.153
	<i>NMAEF</i>	0.322	0.369	0.305	0.215	0.319	0.376	0.321	0.226
Con	<i>NMBF</i>	-0.362	-0.217	-0.252	-0.025	-0.355	-0.209	-0.248	-0.023



(N=16)	<i>NMAEF</i>	0.448	0.455	0.483	0.399	0.427	0.458	0.470	0.394
Tro	<i>NMBF</i>	0.080	-0.808	-0.086	-0.438	0.075	-0.813	-0.090	-0.441
(N=5)	<i>NMAEF</i>	0.423	0.831	0.404	0.569	0.422	0.832	0.399	0.567
Gra	<i>NMBF</i>	0.276	0.015	0.175	0.097	0.294	0.011	0.186	0.110
(N=10)	<i>NMAEF</i>	0.392	0.479	0.307	0.318	0.396	0.467	0.302	0.311
Cro	<i>NMBF</i>	0.297	0.360	0.241	0.282	0.318	0.371	0.255	0.292
(N=11)	<i>NMAEF</i>	0.473	0.541	0.474	0.570	0.485	0.550	0.480	0.576

715 **Table 2:** Performance metrics (*NMBF* and *NMAEF*) for daytime average v_d simulated by the four dry deposition
 716 parameterizations. “Static LAI” is the result from [Clim] run, which uses 1982-2011 AVHRR monthly climatological LAI,
 717 while “Dynamic LAI” is the result from [Clim+LAI], which uses 1982-2011 AVHRR LAI time series. Dec = deciduous
 718 forest, Con = coniferous forest, Tro = tropical rainforest, Gra = grassland, Cro = cropland. *N* indicates the number of
 719 observational datasets involved in that particular land type. The best performing parameterization for each land type has its
 720 performance metrics bolded.

721
 722
 723
 724
 725
 726

727 References

- 728 Ainsworth, E. A., Yendrek, C. R., Sitch, S., Collins, W. J. and Emberson, L. D.: The Effects of Tropospheric Ozone on Net
 729 Primary Productivity and Implications for Climate Change, *Annu. Rev. Plant Biol.*, 63(1), 637–661, doi:10.1146/annurev-
 730 arplant-042110-103829, 2012.
- 731 Altimir, N., Kolari, P., Tuovinen, J.-P., Vesala, T., Bäck, J., Suni, T., Kulmala, M. and Hari, P.: Foliage surface ozone
 732 deposition: a role for surface moisture?, *Biogeosciences Discuss.*, 2, 1739–1793, doi:10.5194/bgd-2-1739-2005, 2006.
- 733 Ashworth, K., Chung, S. H., Griffin, R. J., Chen, J., Forkel, R., Bryan, A. M. and Steiner, A. L.: FORest Canopy Atmosphere
 734 Transfer (FORCAST) 1.0: A 1-D model of biosphere-atmosphere chemical exchange, *Geosci. Model Dev.*, doi:10.5194/gmd-
 735 8-3765-2015, 2015.
- 736 Avnery, S., Mauzerall, D. L., Liu, J. and Horowitz, L. W.: Global crop yield reductions due to surface ozone exposure: 1. Year
 737 2000 crop production losses and economic damage, *Atmos. Environ.*, 45(13), 2284–2296,
 738 doi:10.1016/j.atmosenv.2010.11.045, 2011.
- 739 Baldocchi, D., Falge, E., Gu, L., Olson, R., Hollinger, D., Running, S., Anthoni, P., Bernhofer, C., Davis, K., Evans, R.,



- 740 Fuentes, J., Goldstein, A., Katul, G., Law, B., Lee, X., Malhi, Y., Meyers, T., Munger, W., Oechel, W., Paw, U. K. T.,
741 Pilegaard, K., Schmid, H. P., Valentini, R., Verma, S., Vesala, T., Wilson, K. and Wofsy, S.: FLUXNET: A New Tool to
742 Study the Temporal and Spatial Variability of Ecosystem-Scale Carbon Dioxide, Water Vapor, and Energy Flux Densities,
743 *Bull. Am. Meteorol. Soc.*, doi:10.1175/1520-0477(2001)082<2415:FANTTS>2.3.CO;2, 2001.
- 744 Baldocchi, D. D., Hicks, B. B. and Camara, P.: A canopy stomatal resistance model for gaseous deposition to vegetated
745 surfaces, *Atmos. Environ.*, 21(1), 91–101, doi:10.1016/0004-6981(87)90274-5, 1987.
- 746 Ball, J. T., Woodrow, I. E. and Berry, J. A.: A Model Predicting Stomatal Conductance and its Contribution to the Control of
747 Photosynthesis under Different Environmental Conditions, in *Progress in Photosynthesis Research*, pp. 221–224., 1987.
- 748 Bey, I., Jacob, D. J., Yantosca, R. M., Logan, J. A., Field, B. D., Fiore, A. M., Li, Q., Liu, H. Y., Mickley, L. J. and Schultz,
749 M. G.: Global modeling of tropospheric chemistry with assimilated meteorology: Model description and evaluation, *J.*
750 *Geophys. Res. Atmos.*, 106(D19), 23073–23095, doi:10.1029/2001JD000807, 2001.
- 751 Brook, J. R., Zhang, L., Di-Giovanni, F. and Padro, J.: Description and evaluation of a model of deposition velocities for
752 routine estimates of air pollutant dry deposition over North America. Part I: Model development, *Atmos. Environ.*,
753 doi:10.1016/S1352-2310(99)00250-2, 1999.
- 754 Brown-Steiner, B., Selin, N. E., Prinn, R. G., Monier, E., Tilmes, S., Emmons, L. and Garcia-Menendez, F.: Maximizing ozone
755 signals among chemical, meteorological, and climatological variability, *Atmos. Chem. Phys.*, doi:10.5194/acp-18-8373-2018,
756 2018.
- 757 Centoni, F.: Global scale modelling of ozone deposition processes and interaction between surface ozone and climate change
758 A thesis presented for the degree The University of Edinburgh, University of Edinburgh., 2017.
- 759 Chen, B., Black, T. A., Coops, N. C., Hilker, T., Trofymow, J. A. and Morgenstern, K.: Assessing tower flux footprint
760 climatology and scaling between remotely sensed and eddy covariance measurements, *Boundary-Layer Meteorol.*,
761 doi:10.1007/s10546-008-9339-1, 2009.
- 762 Chen, B., Coops, N. C., Fu, D., Margolis, H. A., Amiro, B. D., Black, T. A., Arain, M. A., Barr, A. G., Bourque, C. P. A.,
763 Flanagan, L. B., Lafleur, P. M., McCaughey, J. H. and Wofsy, S. C.: Characterizing spatial representativeness of flux tower
764 eddy-covariance measurements across the Canadian Carbon Program Network using remote sensing and footprint analysis,
765 *Remote Sens. Environ.*, doi:10.1016/j.rse.2012.06.007, 2012.
- 766 Clifton, O. E., Fiore, A. M., Munger, J. W., Malyshev, S., Horowitz, L. W., Shevliakova, E., Paulot, F., Murray, L. T. and
767 Griffin, K. L.: Interannual variability in ozone removal by a temperate deciduous forest, *Geophys. Res. Lett.*, 44(1), 542–552,
768 doi:10.1002/2016GL070923, 2017.
- 769 Coe, H., Gallagher, M. W., Choularton, T. W. and Dore, C.: Canopy scale measurements of stomatal and cuticular O₃ uptake
770 by sitka spruce, *Atmos. Environ.*, doi:10.1016/1352-2310(95)00034-V, 1995.
- 771 Collatz, G., Ribas-Carbo, M. and Berry, J.: Coupled Photosynthesis-Stomatal Conductance Model for Leaves of C₄ Plants,
772 *Aust. J. Plant Physiol.*, 19(5), 519, doi:10.1071/PP9920519, 1992.
- 773 Collatz, G. J., Ball, J. T., Grivet, C. and Berry, J. A.: Physiological and environmental regulation of stomatal conductance,



- 774 photosynthesis and transpiration: a model that includes a laminar boundary layer, *Agric. For. Meteorol.*, 54(2–4), 107–136,
775 doi:10.1016/0168-1923(91)90002-8, 1991.
- 776 Coyle, M., Nemitz, E., Storeton-West, R., Fowler, D. and Cape, J. N.: Measurements of ozone deposition to a potato canopy,
777 *Agric. For. Meteorol.*, doi:10.1016/j.agrformet.2008.10.020, 2009.
- 778 Droppo, J. G.: Concurrent measurements of ozone dry deposition using eddy correlation and profile flux methods., *J. Geophys.*
779 *Res.*, doi:10.1029/JD090iD01p02111, 1985.
- 780 Ducker, J. A., Holmes, C. D., Keenan, T. F., Fares, S., Goldstein, A. H., Mammarella, I., William Munger, J. and Schnell, J.:
781 Synthetic ozone deposition and stomatal uptake at flux tower sites, *Biogeosciences*, doi:10.5194/bg-15-5395-2018, 2018.
- 782 Emberson, L. D., Wieser, G. and Ashmore, M. R.: Modelling of stomatal conductance and ozone flux of Norway spruce:
783 Comparison with field data, in *Environmental Pollution.*, 2000.
- 784 Fares, S., McKay, M., Holzinger, R. and Goldstein, A. H.: Ozone fluxes in a *Pinus ponderosa* ecosystem are dominated by
785 non-stomatal processes: Evidence from long-term continuous measurements, *Agric. For. Meteorol.*, 150(3), 420–431,
786 doi:10.1016/j.agrformet.2010.01.007, 2010.
- 787 Fares, S., Savi, F., Muller, J., Matteucci, G. and Paoletti, E.: Simultaneous measurements of above and below canopy ozone
788 fluxes help partitioning ozone deposition between its various sinks in a Mediterranean Oak Forest, *Agric. For. Meteorol.*, 198,
789 181–191, doi:10.1016/j.agrformet.2014.08.014, 2014.
- 790 Fares, S., Conte, A. and Chabbi, A.: Ozone flux in plant ecosystems: new opportunities for long-term monitoring networks to
791 deliver ozone-risk assessments, *Environ. Sci. Pollut. Res.*, 1–9, doi:10.1007/s11356-017-0352-0, 2017.
- 792 Farquhar, G. D., Von Caemmerer, S. and Berry, J. A.: A Biochemical Model of Photosynthetic CO₂ Assimilation in Leaves
793 of C₃ Species, *Planta*, 149, 78–90, doi:10.1007/BF00386231, 1980.
- 794 Finkelstein, P. L., Ellestad, T. G., Clarke, J. F., Meyers, T. P., Schwede, D. B., Hebert, E. O. and Neal, J. A.: Ozone and sulfur
795 dioxide dry deposition to forests: Observations and model evaluation, *J. Geophys. Res. Atmos.*, doi:10.1029/2000JD900185,
796 2000.
- 797 Fiore, A. M., Oberman, J. T., Lin, M. Y., Zhang, L., Clifton, O. E., Jacob, D. J., Naik, V., Horowitz, L. W., Pinto, J. P. and
798 Milly, G. P.: Estimating North American background ozone in U.S. surface air with two independent global models:
799 Variability, uncertainties, and recommendations, *Atmos. Environ.*, doi:10.1016/j.atmosenv.2014.07.045, 2014.
- 800 Foken, T.: 50 years of the Monin-Obukhov similarity theory, *Boundary-Layer Meteorol.*, doi:10.1007/s10546-006-9048-6,
801 2006.
- 802 Folberth, C., Skalský, R., Moltchanova, E., Balkovič, J., Azevedo, L. B., Obersteiner, M. and Van Der Velde, M.: Uncertainty
803 in soil data can outweigh climate impact signals in global crop yield simulations, *Nat. Commun.*, doi:10.1038/ncomms11872,
804 2016.
- 805 Fowler, D., Flechard, C., Cape, J. N., Storeton-West, R. L. and Coyle, M.: Measurements of ozone deposition to vegetation
806 quantifying the flux, the stomatal and non-stomatal components, *Water. Air. Soil Pollut.*, doi:10.1023/A:1012243317471,
807 2001.



- 808 Fowler, D., Nemitz, E., Misztal, P., di Marco, C., Skiba, U., Ryder, J., Helfter, C., Neil Cape, J., Owen, S., Dorsey, J.,
809 Gallagher, M. W., Coyle, M., Phillips, G., Davison, B., Langford, B., MacKenzie, R., Muller, J., Siong, J., Dari-Salisburgo,
810 C., di Carlo, P., Aruffo, E., Giammaria, F., Pyle, J. A. and Nicholas Hewitt, C.: Effects of land use on surface-atmosphere
811 exchanges of trace gases and energy in Borneo: Comparing fluxes over oil palm plantations and a rainforest, *Philos. Trans. R.*
812 *Soc. B Biol. Sci.*, doi:10.1098/rstb.2011.0055, 2011.
- 813 Franks, P. J., Adams, M. A., Amthor, J. S., Barbour, M. M., Berry, J. A., Ellsworth, D. S., Farquhar, G. D., Ghannoum, O.,
814 Lloyd, J., McDowell, N., Norby, R. J., Tissue, D. T. and von Caemmerer, S.: Sensitivity of plants to changing atmospheric
815 CO₂ concentration: From the geological past to the next century, *New Phytol.*, 197(4), 1077–1094, doi:10.1111/nph.12104,
816 2013.
- 817 Fu, Y. and Tai, A. P. K.: Impact of climate and land cover changes on tropospheric ozone air quality and public health in East
818 Asia between 1980 and 2010, *Atmos. Chem. Phys.*, 15(17), 10093–10106, doi:10.5194/acp-15-10093-2015, 2015.
- 819 Ganzeveld, L., Bouwman, L., Stehfest, E., van Vuuren, D. P., Eickhout, B. and Lelieveld, J.: Impact of future land use and
820 land cover changes on atmospheric chemistry-climate interactions, *J. Geophys. Res.*, 115(D23), D23301,
821 doi:10.1029/2010JD014041, 2010.
- 822 Gao, W. and Wesely, M. L.: Modeling gaseous dry deposition over regional scales with satellite observations-I. Model
823 development, *Atmos. Environ.*, 29(6), 727–737, doi:10.1016/1352-2310(94)00284-R, 1995.
- 824 Geddes, J. A. and Martin, R. V.: Global deposition of total reactive nitrogen oxides from 1996 to 2014 constrained with satellite
825 observations of NO₂ columns, *Atmos. Chem. Phys.*, doi:10.5194/acp-17-10071-2017, 2017.
- 826 Geddes, J. A., Heald, C. L., Silva, S. J. and Martin, R. V.: Land cover change impacts on atmospheric chemistry: Simulating
827 projected large-scale tree mortality in the United States, *Atmos. Chem. Phys.*, 16(4), 2323–2340, doi:10.5194/acp-16-2323-
828 2016, 2016.
- 829 Gelaro, R., McCarty, W., Suárez, M. J., Todling, R., Molod, A., Takacs, L., Randles, C. A., Darmenov, A., Bosilovich, M. G.,
830 Reichle, R., Wargan, K., Coy, L., Cullather, R., Draper, C., Akella, S., Buchard, V., Conaty, A., da Silva, A. M., Gu, W., Kim,
831 G. K., Koster, R., Lucchesi, R., Merkova, D., Nielsen, J. E., Partyka, G., Pawson, S., Putman, W., Rienecker, M., Schubert, S.
832 D., Sienkiewicz, M. and Zhao, B.: The modern-era retrospective analysis for research and applications, version 2 (MERRA-
833 2), *J. Clim.*, 30(14), 5419–5454, doi:10.1175/JCLI-D-16-0758.1, 2017.
- 834 Gerosa, G., Vitale, M., Finco, A., Manes, F., Denti, A. B. and Cieslik, S.: Ozone uptake by an evergreen Mediterranean Forest
835 (*Quercus ilex*) in Italy. Part I: Micrometeorological flux measurements and flux partitioning, *Atmos. Environ.*, 39(18), 3255–
836 3266, doi:10.1016/j.atmosenv.2005.01.056, 2005.
- 837 Gerosa, G., Marzuoli, R., Monteleone, B., Chiesa, M. and Finco, A.: Vertical ozone gradients above forests. Comparison of
838 different calculation options with direct ozone measurements above a mature forest and consequences for ozone risk
839 assessment, *Forests*, 8(9), doi:10.3390/f8090337, 2017.
- 840 Hardacre, C., Wild, O. and Emberson, L.: An evaluation of ozone dry deposition in global scale chemistry climate models,
841 *Atmos. Chem. Phys.*, 15(11), 6419–6436, doi:10.5194/acp-15-6419-2015, 2015.



- 842 Heald, C. L. and Geddes, J. A.: The impact of historical land use change from 1850 to 2000 on secondary particulate matter
843 and ozone, *Atmos. Chem. Phys.*, doi:10.5194/acp-16-14997-2016, 2016.
- 844 Hole, L. R., Semb, A. and Tørseth, K.: Ozone deposition to a temperate coniferous forest in Norway; gradient method
845 measurements and comparison with the EMEP deposition module, in *Atmospheric Environment.*, 2004.
- 846 Hoshika, Y., Carriero, G., Feng, Z., Zhang, Y. and Paoletti, E.: Determinants of stomatal sluggishness in ozone-exposed
847 deciduous tree species, *Sci. Total Environ.*, 481(1), 453–458, doi:10.1016/j.scitotenv.2014.02.080, 2014.
- 848 Hu, L., Jacob, D. J., Liu, X., Zhang, Y., Zhang, L., Kim, P. S., Sulprizio, M. P. and Yantosca, R. M.: Global budget of
849 tropospheric ozone: Evaluating recent model advances with satellite (OMI), aircraft (IAGOS), and ozonesonde observations,
850 *Atmos. Environ.*, 167, 323–334, doi:10.1016/j.atmosenv.2017.08.036, 2017.
- 851 Huang, L., McDonald-Buller, E. C., McGaughey, G., Kimura, Y. and Allen, D. T.: The impact of drought on ozone dry
852 deposition over eastern Texas, *Atmos. Environ.*, 127, 176–186, doi:10.1016/j.atmosenv.2015.12.022, 2016.
- 853 Jacob, D. J. and Wofsy, S. C.: Budgets of Reactive Nitrogen, Hydrocarbons, and Ozone Over the Amazon Forest during the
854 Wet Season, *J. Geophys. Res.*, 95, 16737–16754, doi:10.1029/JD095iD10p16737, 1990.
- 855 Jacob, D. J., Fan, S.-M., Wofsy, S. C., Spiro, P. A., Bakwin, P. S., Ritter, J. A., Browell, E. V., Gregory, G. L., Fitzjarrald, D.
856 R. and Moore, K. E.: Deposition of ozone to tundra, *J. Geophys. Res.*, doi:10.1029/91JD02696, 1992.
- 857 Jarvis, P. G.: The Interpretation of the Variations in Leaf Water Potential and Stomatal Conductance Found in Canopies in the
858 Field, *Philos. Trans. R. Soc. B Biol. Sci.*, 273(927), 593–610, doi:10.1098/rstb.1976.0035, 1976.
- 859 Jerrett, M., Burnett, R. T., Pope, C. A., Ito, K., Thurston, G., Krewski, D., Shi, Y., Calle, E. and Thun, M.: Long-Term Ozone
860 Exposure and Mortality, *N. Engl. J. Med.*, 360(11), 1085–1095, doi:10.1056/NEJMoa0803894, 2009.
- 861 Jiang, C., Ryu, Y., Fang, H., Myneni, R., Claverie, M. and Zhu, Z.: Inconsistencies of interannual variability and trends in
862 long-term satellite leaf area index products, *Glob. Chang. Biol.*, doi:10.1111/gcb.13787, 2017.
- 863 Junninen, H., Lauri, A., Keronen, P., Aalto, P., Hiltunen, V., Hari, P. and Kulmala, M.: Smart-SMEAR: On-line data
864 exploration and visualization tool for SMEAR stations, *Boreal Environ. Res.*, 14(4), 447–457, 2009.
- 865 Kammer, J., Lamaud, E., Bonnefond, J. M., Garrigou, D., Flaud, P. M., Perraudin, E. and Villenave, E.: Ozone production in
866 a maritime pine forest in water-stressed conditions, *Atmos. Environ.*, 197, 131–140, doi:10.1016/j.atmosenv.2018.10.021,
867 2019.
- 868 Kattge, J. and Knorr, W.: Temperature acclimation in a biochemical model of photosynthesis: A reanalysis of data from 36
869 species, *Plant, Cell Environ.*, 30(9), 1176–1190, doi:10.1111/j.1365-3040.2007.01690.x, 2007.
- 870 Kavassalis, S. C. and Murphy, J. G.: Understanding ozone-meteorology correlations: A role for dry deposition, *Geophys. Res.*
871 *Let.*, 44(6), 2922–2931, doi:10.1002/2016GL071791, 2017.
- 872 Keeling, C. D., Stephen, C., Piper, S. C., Bacastow, R. B., Wahlen, M., Whorf, T. P., Heimann, M. and Meijer, H. a.: Exchanges
873 of atmospheric CO₂ and ¹³CO₂ with the terrestrial biosphere and oceans from 1978 to 2000, *Glob. Asp. SIO Ref. Ser. Scripps*
874 *Inst. Ocean. San Diego*, doi:10.1007/b138533, 2001.
- 875 Keronen, P., Reissell, a, Rannik, Ü., Pohja, T., Siivola, E., Hiltunen, V., Hari, P., Kulmala, M. and Vesala, T.: Ozone flux



- 876 measurements over a Scots pine forest using eddy covariance method: Performance evaluation and comparison with flux-
877 profile method, *Boreal Environ. Res.*, 8(4), 425–443 [online] Available from:
878 [http://www.scopus.com/inward/record.url?eid=2-s2.0-](http://www.scopus.com/inward/record.url?eid=2-s2.0-0347884158&partnerID=40&md5=4ad114fb52c557d36cc8a0ec1ab8bb7e)
879 [0347884158&partnerID=40&md5=4ad114fb52c557d36cc8a0ec1ab8bb7e](http://www.scopus.com/inward/record.url?eid=2-s2.0-0347884158&partnerID=40&md5=4ad114fb52c557d36cc8a0ec1ab8bb7e), 2003.
- 880 Kharol, S. K., Shephard, M. W., Mclinden, C. A., Zhang, L., Sioris, C. E., O'Brien, J. M., Vet, R., Cady-Pereira, K. E., Hare,
881 E., Siemons, J. and Krotkov, N. A.: Dry Deposition of Reactive Nitrogen From Satellite Observations of Ammonia and
882 Nitrogen Dioxide Over North America, *Geophys. Res. Lett.*, doi:10.1002/2017GL075832, 2018.
- 883 Kurpius, M. R., McKay, M. and Goldstein, A. H.: Annual ozone deposition to a Sierra Nevada ponderosa pine plantation,
884 *Atmos. Environ.*, doi:10.1016/S1352-2310(02)00423-5, 2002.
- 885 Lamaud, E., Brunet, Y., Labatut, A., Lopez, A., Fontan, J. and Druilhet, A.: The Landes experiment: Biosphere-atmosphere
886 exchanges of ozone and aerosol particles above a pine forest, *J. Geophys. Res.*, doi:10.1029/94JD00668, 1994.
- 887 Lamaud, E., Carrara, A., Brunet, Y., Lopez, A. and Druilhet, A.: Ozone fluxes above and within a pine forest canopy in dry
888 and wet conditions, *Atmos. Environ.*, 36(1), 77–88, doi:10.1016/S1352-2310(01)00468-X, 2002.
- 889 Lawrence, P. J. and Chase, T. N.: Representing a new MODIS consistent land surface in the Community Land Model (CLM
890 3.0), *J. Geophys. Res. Biogeosciences*, 112(1), doi:10.1029/2006JG000168, 2007.
- 891 Li, D., Bou-Zeid, E., Barlage, M., Chen, F. and Smith, J. A.: Development and evaluation of a mosaic approach in the WRF-
892 Noah framework, *J. Geophys. Res. Atmos.*, 118(21), 11918–11935, doi:10.1002/2013JD020657, 2013.
- 893 Li, Q., Gabay, M., Rubin, Y., Fredj, E. and Tas, E.: Measurement-based investigation of ozone deposition to vegetation under
894 the effects of coastal and photochemical air pollution in the Eastern Mediterranean, *Sci. Total Environ.*,
895 doi:10.1016/j.scitotenv.2018.07.037, 2018.
- 896 Lombardozzi, D., Sparks, J. P., Bonan, G. and Levis, S.: Ozone exposure causes a decoupling of conductance and
897 photosynthesis: Implications for the Ball-Berry stomatal conductance model, *Oecologia*, 169(3), 651–659,
898 doi:10.1007/s00442-011-2242-3, 2012.
- 899 Lombardozzi, D., Levis, S., Bonan, G., Hess, P. G. and Sparks, J. P.: The influence of chronic ozone exposure on global carbon
900 and water cycles, *J. Clim.*, 28(1), 292–305, doi:10.1175/JCLI-D-14-00223.1, 2015.
- 901 Malhi, Y., Roberts, J. T., Betts, R. A., Killeen, T. J., Li, W. and Nobre, C. A.: Climate change, deforestation, and the fate of
902 the Amazon, *Science* (80-.), doi:10.1126/science.1146961, 2008.
- 903 Mao, J., Paulot, F., Jacob, D. J., Cohen, R. C., Crouse, J. D., Wennberg, P. O., Keller, C. A., Hudman, R. C., Barkley, M. P.
904 and Horowitz, L. W.: Ozone and organic nitrates over the eastern United States: Sensitivity to isoprene chemistry, *J. Geophys.*
905 *Res. Atmos.*, 118(19), 11256–11268, doi:10.1002/jgrd.50817, 2013.
- 906 Matsuda, K., Watanabe, I., Wingpud, V., Theramongkol, P., Khummongkol, P., Wangwongwatana, S. and Totsuka, T.: Ozone
907 dry deposition above a tropical forest in the dry season in northern Thailand, *Atmos. Environ.*, 39(14), 2571–2577,
908 doi:10.1016/j.atmosenv.2005.01.011, 2005.
- 909 McGrath, J. M., Betzelberger, A. M., Wang, S., Shook, E., Zhu, X.-G., Long, S. P. and Ainsworth, E. A.: An analysis of ozone



- 910 damage to historical maize and soybean yields in the United States, *Proc. Natl. Acad. Sci.*, 112(46), 14390–14395,
911 doi:10.1073/pnas.1509777112, 2015.
- 912 Mészáros, R., Horváth, L., Weidinger, T., Neftel, A., Nemitz, E., Dämmgen, U., Cellier, P. and Loubet, B.: Measurement and
913 modelling ozone fluxes over a cut and fertilized grassland, *Biogeosciences*, doi:10.1029/2002GL016785.
- 914 Meyers, T. P., Finkelstein, P., Clarke, J., Ellestad, T. G. and Sims, P. F.: A multilayer model for inferring dry deposition using
915 standard meteorological measurements, *J. Geophys. Res.*, 103(98), 22645, doi:10.1029/98JD01564, 1998.
- 916 Mikkelsen, T. N., Ro-Poulsen, H., Hovmand, M. F., Jensen, N. O., Pilegaard, K. and Egeløv, A. H.: Five-year measurements
917 of ozone fluxes to a Danish Norway spruce canopy, in *Atmospheric Environment.*, 2004.
- 918 Muller, J. B. A., Percival, C. J., Gallagher, M. W., Fowler, D., Coyle, M. and Nemitz, E.: Sources of uncertainty in eddy
919 covariance ozone flux measurements made by dry chemiluminescence fast response analysers, *Atmos. Meas. Tech.*,
920 doi:10.5194/amt-3-163-2010, 2010.
- 921 Munger, J. W., Wofsy, S. C., Bakwin, P. S., Fan, S.-M., Goulden, M. L., Daube, B. C., Goldstein, A. H., Moore, K. E. and
922 Fitzjarrald, D. R.: Atmospheric deposition of reactive nitrogen oxides and ozone in a temperate deciduous forest and a subarctic
923 woodland 1. Measurements and mechanisms, *J. Geophys. Res.*, 101657(20), 639–12, doi:10.1029/96JD00230, 1996.
- 924 Myneni, R. B., Hoffman, S., Knyazikhin, Y., Privette, J. L., Glassy, J., Tian, Y., Wang, Y., Song, X., Zhang, Y., Smith, G. R.,
925 Lotsch, A., Friedl, M., Morisette, J. T., Votava, P., Nemani, R. R. and Running, S. W.: Global products of vegetation leaf area
926 and fraction absorbed PAR from year one of MODIS data, *Remote Sens. Environ.*, 83(1–2), 214–231, doi:10.1016/S0034-
927 4257(02)00074-3, 2002.
- 928 Nowlan, C. R., Martin, R. V., Philip, S., Lamsal, L. N., Krotkov, N. A., Marais, E. A., Wang, S. and Zhang, Q.: Global dry
929 deposition of nitrogen dioxide and sulfur dioxide inferred from space-based measurements, *Global Biogeochem. Cycles*,
930 doi:10.1002/2014GB004805, 2014.
- 931 Oleson, K. W., Lawrence, D. M., Bonan, G. B., Drewniak, B., Huang, M., Koven, C. D., Levis, S., Li, F., Riley, J., Subin, Z.
932 M., Swenson, S. C., Thornton, P. E., Bozbiyik, A., Fisher, R. A., Heald, C. L., Kluzek, E., Lamarque, J.-F., Lawrence, P. J.,
933 Leung, L. R., Lipscomb, W., Muszala, S., Ricciuto, D. M., Sacks, W. J., Sun, Y., Tang, J. and Yang, Z.-L.: Technical
934 Description of version 4.5 of the Community Land Model (CLM)., 2013.
- 935 Olson, D. M., Dinerstein, E., Wikramanayake, E. D., Burgess, N. D., Powell, G. V. N., Underwood, E. C., D'Amico, J. A.,
936 Itoua, I., Strand, H. E., Morrison, J. C., Loucks, C. J., Allnutt, T. F., Ricketts, T. H., Kura, Y., Lamoreux, J. F., Wettengel, W.
937 W., Hedao, P. and Kassem, K. R.: Terrestrial Ecoregions of the World: A New Map of Life on Earth, *Bioscience*,
938 doi:10.1641/0006-3568(2001)051[0933:TEOTWA]2.0.CO;2, 2001.
- 939 Padro, J., den Hartog, G. and Neumann, H. H.: An investigation of the ADOM dry deposition module using summertime
940 O₃ measurements above a deciduous forest, *Atmos. Environ. Part A, Gen. Top.*, doi:10.1016/0960-1686(91)90027-5, 1991.
- 941 Padro, J., Massman, W. J., Shaw, R. H., Delany, A. and Oncley, S. P.: A comparison of some aerodynamic resistance methods
942 using measurements over cotton and grass from the 1991 California ozone deposition experiment, *Boundary-Layer Meteorol.*,
943 doi:10.1007/BF00712174, 1994.



- 944 Paulson, C. A.: The Mathematical Representation of Wind Speed and Temperature Profiles in the Unstable Atmospheric
945 Surface Layer, *J. Appl. Meteorol.*, doi:10.1175/1520-0450(1970)009<0857:tmrows>2.0.co;2, 2002.
- 946 Pilegaard, K., Hummelshøj, P. and Jensen, N. O.: Fluxes of ozone and nitrogen dioxide measured by eddy correlation over a
947 harvested wheat field, *Atmos. Environ.*, doi:10.1016/S1352-2310(97)00194-5, 1998.
- 948 Pio, C. ., Feliciano, M. ., Vermeulen, A. . and Sousa, E. .: Seasonal variability of ozone dry deposition under southern European
949 climate conditions, in Portugal, *Atmos. Environ.*, doi:10.1016/S1352-2310(99)00276-9, 2000.
- 950 Pleim, J. and Ran, L.: Surface flux modeling for air quality applications, *Atmosphere (Basel)*, 2(3), 271–302,
951 doi:10.3390/atmos2030271, 2011.
- 952 Potier, E., Ogée, J., Jouanguy, J., Lamaud, E., Stella, P., Personne, E., Durand, B., Mascher, N. and Loubet, B.: Multilayer
953 modelling of ozone fluxes on winter wheat reveals large deposition on wet senescing leaves, *Agric. For. Meteorol.*, 211–212,
954 58–71, doi:10.1016/j.agrformet.2015.05.006, 2015.
- 955 Potier, E., Loubet, B., Durand, B., Flura, D., Bourdat-Deschamps, M., Ciuraru, R. and Ogée, J.: Chemical reaction rates of
956 ozone in water infusions of wheat, beech, oak and pine leaves of different ages, *Atmos. Environ.*, 151, 176–187,
957 doi:10.1016/j.atmosenv.2016.11.069, 2017.
- 958 R core team: R: A language and environment for statistical computing., *R Found. Stat. Comput. Vienna, Austria.*,
959 doi:http://www.R-project.org/, 2017.
- 960 Ran, L., Pleim, J., Song, C., Band, L., Walker, J. T. and Binkowski, F. S.: A photosynthesis-based two-leaf canopy stomatal
961 conductance model for meteorology and air quality modeling with WRF/CMAQ PX LSM, *J. Geophys. Res.*, 122(3), 1930–
962 1952, doi:10.1002/2016JD025583, 2017a.
- 963 Ran, L., Pleim, J., Song, C., Band, L., Walker, J. T. and Binkowski, F. S.: A photosynthesis-based two-leaf canopy stomatal
964 conductance model for meteorology and air quality modeling with WRF/CMAQ PX LSM, *J. Geophys. Res.*, 122(3), 1930–
965 1952, doi:10.1002/2016JD025583, 2017b.
- 966 Rannik, Ü., Altimir, N., Mammarella, I., Bäck, J., Rinne, J., Ruuskanen, T. M., Hari, P., Vesala, T. and Kulmala, M.: Ozone
967 deposition into a boreal forest over a decade of observations: Evaluating deposition partitioning and driving variables, *Atmos.*
968 *Chem. Phys.*, 12(24), 12165–12182, doi:10.5194/acp-12-12165-2012, 2012.
- 969 Reich, P. B.: Quantifying plant response to ozone: a unifying theory, *Tree Physiol.*, 3(0), 63–91, doi:10.1093/treephys/3.1.63,
970 1987.
- 971 Rienecker, M. M. and Coauthors: The GEOS-5 Data Assimilation System—Documentation of versions 5.0.1 and 5.1.0, and
972 5.2.0, *NASA Tech. Rep. Ser. Glob. Model. Data Assim. NASA/TM-2008-104606*, doi:10.2759/32049, 2008.
- 973 Rigden, A. J. and Salvucci, G. D.: Stomatal response to humidity and CO₂ implicated in recent decline in US evaporation,
974 *Glob. Chang. Biol.*, doi:10.1111/gcb.13439, 2017.
- 975 Rummel, U., Ammann, C., Kirkman, G. A., Moura, M. A. L., Foken, T., Andreae, M. O. and Meixner, F. X.: Seasonal variation
976 of ozone deposition to a tropical rain forest in southwest Amazonia, *Atmos. Chem. Phys.*, doi:10.5194/acp-7-5415-2007, 2007.
- 977 Sadiq, M., Tai, A. P. K., Lombardozzi, D. and Val Martin, M.: Effects of ozone-vegetation coupling on surface ozone air



- 978 quality via biogeochemical and meteorological feedbacks, *Atmos. Chem. Phys.*, 17(4), 3055–3066, doi:10.5194/acp-17-3055-
979 2017, 2017.
- 980 Sanderson, M. G., Collins, W. J., Hemming, D. L. and Betts, R. A.: Stomatal conductance changes due to increasing carbon
981 dioxide levels: Projected impact on surface ozone levels, *Tellus, Ser. B Chem. Phys. Meteorol.*, 59(3), 404–411,
982 doi:10.1111/j.1600-0889.2007.00277.x, 2007.
- 983 Sen, P. K.: Estimates of the Regression Coefficient Based on Kendall's Tau, *J. Am. Stat. Assoc.*,
984 doi:10.1080/01621459.1968.10480934, 1968.
- 985 Silva, S. J. and Heald, C. L.: Investigating Dry Deposition of Ozone to Vegetation, *J. Geophys. Res. Atmos.*, 123(1), 559–573,
986 doi:10.1002/2017JD027278, 2018.
- 987 Silva, S. J., Heald, C. L., Ravela, S., Mammarella, I. and Munger, J. W.: A Deep Learning Parameterization for Ozone Dry
988 Deposition Velocities, *Geophys. Res. Lett.*, 1–7, doi:10.1029/2018GL081049, 2019.
- 989 Simpson, D., Benedictow, A., Berge, H., Bergström, R., Emberson, L. D., Fagerli, H., Flechard, C. R., Hayman, G. D., Gauss,
990 M., Jonson, J. E., Jenkin, M. E., Nyíri, A., Richter, C., Semeena, V. S., Tsyro, S., Tuovinen, J.-P., Valdebenito, A. and Wind,
991 P.: The EMEP MSC-W chemical transport model – technical description, *Atmos. Chem. Phys. Atmos. Chem. Phys.*, 12, 7825–
992 7865, doi:10.5194/acp-12-7825-2012, 2012.
- 993 Sitch, S., Cox, P. M., Collins, W. J. and Huntingford, C.: Indirect radiative forcing of climate change through ozone effects on
994 the land-carbon sink, *Nature*, 448(7155), 791–794, doi:10.1038/nature06059, 2007.
- 995 Song-Miao, F., Wofsy, S. C., Bakwin, P. S., Jacob, D. J. and Fitzjarrald, D. R.: Atmosphere-biosphere exchange of CO₂ and
996 O₃ in the central Amazon forest, *J. Geophys. Res.*, doi:10.1029/JD095iD10p16851, 1990.
- 997 Stella, P., Loubet, B., Lamaud, E., Laville, P. and Cellier, P.: Ozone deposition onto bare soil: A new parameterisation, *Agric.
998 For. Meteorol.*, 151(6), 669–681, doi:10.1016/j.agrformet.2011.01.015, 2011a.
- 999 Stella, P., Personne, E., Loubet, B., Lamaud, E., Ceschia, E., B??ziat, P., Bonnefond, J. M., Irvine, M., Keravec, P., Mascher,
1000 N. and Cellier, P.: Predicting and partitioning ozone fluxes to maize crops from sowing to harvest: The Surf atm-O₃ model,
1001 *Biogeosciences*, 8(10), 2869–2886, doi:10.5194/bg-8-2869-2011, 2011b.
- 1002 Stocker, D. W., Stedman, D. H., Zeller, K. F., Massman, W. J. and Fox, D. G.: Fluxes of nitrogen oxides and ozone measured
1003 by eddy correlation over a shortgrass prairie, *J. Geophys. Res.*, doi:10.1029/93JD00871, 1993.
- 1004 Sun, S., Moravek, A., Trebs, I., Kesselmeier, J. and Sörgel, M.: Investigation of the influence of liquid surface films on O₃
1005 and PAN deposition to plant leaves coated with organic/inorganic solution, *J. Geophys. Res. Atmos.*, 121(23), 14,239–14,256,
1006 doi:10.1002/2016JD025519, 2016.
- 1007 Sun, Y., Gu, L. and Dickinson, R. E.: A numerical issue in calculating the coupled carbon and water fluxes in a climate model,
1008 *J. Geophys. Res. Atmos.*, doi:10.1029/2012JD018059, 2012.
- 1009 Tai, A. P. K., Martin, M. V. and Heald, C. L.: Threat to future global food security from climate change and ozone air pollution,
1010 *Nat. Clim. Chang.*, 4(9), 817–821, doi:10.1038/nclimate2317, 2014.
- 1011 Travis, K. R., Jacob, D. J., Fisher, J. A., Kim, P. S., Marais, E. A., Zhu, L., Yu, K., Miller, C. C., Yantosca, R. M., Sulprizio,



- 1012 M. P., Thompson, A. M., Wennberg, P. O., Crounse, J. D., St Clair, J. M., Cohen, R. C., Laughner, J. L., Dibb, J. E., Hall, S.
1013 R., Ullmann, K., Wolfe, G. M., Pollack, I. B., Peischl, J., Neuman, J. A. and Zhou, X.: Why do models overestimate surface
1014 ozone in the Southeast United States?, *Atmos. Chem. Phys.*, 16(21), 13561–13577, doi:10.5194/acp-16-13561-2016, 2016.
- 1015 Turnipseed, A. A., Burns, S. P., Moore, D. J. P., Hu, J., Guenther, A. B. and Monson, R. K.: Controls over ozone deposition
1016 to a high elevation subalpine forest, *Agric. For. Meteorol.*, doi:10.1016/j.agrformet.2009.04.001, 2009.
- 1017 Val Martin, M., Heald, C. L. and Arnold, S. R.: Coupling dry deposition to vegetation phenology in the {Community} {Earth}
1018 {System} {Model}: {Implications} for the simulation of surface {O} ₃, *Geophys. Res. Lett.*, 41(8), 2988–2996,
1019 doi:10.1002/2014GL059651, 2014.
- 1020 Wang, Y., Jacob, D. J. and Logan, J. A.: Global simulation of tropospheric O₃-NO_x-hydrocarbon chemistry: 1. Model
1021 formulation, *J. Geophys. Res. Atmos.*, 103(D9), 10713–10725, doi:10.1029/98JD00158, 1998.
- 1022 Wesely, M. L.: Parameterization of surface resistances to gaseous dry deposition in regional-scale numerical models, *Atmos.*
1023 *Environ.*, 41(SUPPL.), 52–63, doi:10.1016/j.atmosenv.2007.10.058, 1989.
- 1024 Wesely, M. L. and Hicks, B. B.: Some Factors that Affect the Deposition Rates of Sulfur Dioxide and Similar Gases on
1025 Vegetation, *J. Air Pollut. Control Assoc.*, 27(11), 1110–1116, doi:10.1080/00022470.1977.10470534, 1977.
- 1026 Wesely, M. L. and Hicks, B. B.: A review of the current status of knowledge on dry deposition, *Atmos. Environ.*, 34(12–14),
1027 2261–2282, doi:10.1016/S1352-2310(99)00467-7, 2000.
- 1028 Wild, O.: Modelling the global tropospheric ozone budget: exploring the variability in current models, *Atmos. Chem. Phys.*,
1029 7(10), 2643–2660, doi:10.5194/acp-7-2643-2007, 2007.
- 1030 Wittig, V. E., Ainsworth, E. A. and Long, S. P.: To what extent do current and projected increases in surface ozone affect
1031 photosynthesis and stomatal conductance of trees? A meta-analytic review of the last 3 decades of experiments, *Plant, Cell*
1032 *Environ.*, 30(9), 1150–1162, doi:10.1111/j.1365-3040.2007.01717.x, 2007.
- 1033 Wolfe, G. M., Thornton, J. A., McKay, M. and Goldstein, A. H.: Forest-atmosphere exchange of ozone: Sensitivity to very
1034 reactive biogenic VOC emissions and implications for in-canopy photochemistry, *Atmos. Chem. Phys.*, doi:10.5194/acp-11-
1035 7875-2011, 2011.
- 1036 Wong, A. Y. H., Tai, A. P. K. and Ip, Y.-Y.: Attribution and Statistical Parameterization of the Sensitivity of Surface Ozone
1037 to Changes in Leaf Area Index Based On a Chemical Transport Model, *J. Geophys. Res. Atmos.*, 1–16,
1038 doi:10.1002/2017JD027311, 2018.
- 1039 Wu, Z., Wang, X., Chen, F., Turnipseed, A. A., Guenther, A. B., Niyogi, D., Charusombat, U., Xia, B., William Munger, J.
1040 and Alapaty, K.: Evaluating the calculated dry deposition velocities of reactive nitrogen oxides and ozone from two community
1041 models over a temperate deciduous forest, *Atmos. Environ.*, 45(16), 2663–2674, doi:10.1016/j.atmosenv.2011.02.063, 2011.
- 1042 Wu, Z., Staebler, R., Vet, R. and Zhang, L.: Dry deposition of O₃ and SO₂ estimated from gradient measurements above a
1043 temperate mixed forest, *Environ. Pollut.*, 210, 202–210, doi:10.1016/j.envpol.2015.11.052, 2016.
- 1044 Wu, Z., Schwede, D. B., Vet, R., Walker, J. T., Shaw, M., Staebler, R. and Zhang, L.: Evaluation and intercomparison of five
1045 North American dry deposition algorithms at a mixed forest site, *J. Adv. Model. Earth Syst.*, 1–16,



- 1046 doi:10.1029/2017MS001231, 2018.
- 1047 Wu, Z. Y., Zhang, L., Wang, X. M. and Munger, J. W.: A modified micrometeorological gradient method for estimating
1048 O₃ dry depositions over a forest canopy, *Atmos. Chem. Phys.*, 15(13), 7487–7496, doi:10.5194/acp-
1049 15-7487-2015, 2015.
- 1050 Young, P. J., Archibald, A. T., Bowman, K. W., Lamarque, J.-F., Naik, V., Stevenson, D. S., Tilmes, S., Voulgarakis, A.,
1051 Wild, O., Bergmann, D., Cameron-Smith, P., Cionni, I., Collins, W. J., Dalsøren, S. B., Doherty, R. M., Eyring, V., Faluvegi,
1052 G., Horowitz, L. W., Josse, B., Lee, Y. H., MacKenzie, I. A., Nagashima, T., Plummer, D. A., Righi, M., Rumbold, S. T.,
1053 Skeie, R. B., Shindell, D. T., Strode, S. A., Sudo, K., Szopa, S. and Zeng, G.: Pre-industrial to end 21st century projections of
1054 tropospheric ozone from the Atmospheric Chemistry and Climate Model Intercomparison Project (ACCMIP), *Atmos. Chem.*
1055 *Phys.*, doi:10.5194/acp-13-2063-2013, 2013.
- 1056 Yu, S., Eder, B., Dennis, R., Chu, S.-H. and Schwartz, S. E.: New unbiased symmetric metrics for evaluation of air quality
1057 models, *Atmos. Sci. Lett.*, doi:10.1002/asl.125, 2006.
- 1058 Zhang, L., Moran, M. D. and Brook, J. R.: A comparison of models to estimate in-canopy photosynthetically active radiation
1059 and their influence on canopy stomatal resistance, *Atmos. Environ.*, doi:10.1016/S1352-2310(01)00225-4, 2001.
- 1060 Zhang, L., Brook, J. R. and Vet, R.: On ozone dry deposition - With emphasis on non-stomatal uptake and wet canopies,
1061 *Atmos. Environ.*, 36(30), 4787–4799, doi:10.1016/S1352-2310(02)00567-8, 2002.
- 1062 Zhang, L., Brook, J. R. and Vet, R.: A revised parameterization for gaseous dry deposition in air-quality models, *Atmos. Chem.*
1063 *Phys. Discuss.*, 3(2), 1777–1804, doi:10.5194/acpd-3-1777-2003, 2003.
- 1064 Zhang, L., Vet, R., O'Brien, J. M., Mihele, C., Liang, Z. and Wiebe, A.: Dry deposition of individual nitrogen species at eight
1065 Canadian rural sites, *J. Geophys. Res. Atmos.*, doi:10.1029/2008JD010640, 2009.
- 1066 Zhang, L., Jacob, D. J., Liu, X., Logan, J. A., Chance, K., Eldering, A. and Bojkov, B. R.: Intercomparison methods for satellite
1067 measurements of atmospheric composition: Application to tropospheric ozone from TES and OMI, *Atmos. Chem. Phys.*,
1068 10(10), 4725–4739, doi:10.5194/acp-10-4725-2010, 2010.
- 1069 Zhang, L., Jacob, D. J., Knipping, E. M., Kumar, N., Munger, J. W., Carouge, C. C., Van Donkelaar, A., Wang, Y. X. and
1070 Chen, D.: Nitrogen deposition to the United States: Distribution, sources, and processes, *Atmos. Chem. Phys.*,
1071 doi:10.5194/acp-12-4539-2012, 2012.
- 1072 Zhou, P., Ganzeveld, L., Rannik, U., Zhou, L., Gierens, R., Taipale, D., Mammarella, I. and Boy, M.: Simulating ozone dry
1073 deposition at a boreal forest with a multi-layer canopy deposition model, *Atmos. Chem. Phys.*, 17(2), 1361–1379,
1074 doi:10.5194/acp-17-1361-2017, 2017.
- 1075 Zhou, S. S., Tai, A. P. K., Sun, S., Sadiq, M., Heald, C. L. and Geddes, J. A.: Coupling between surface ozone and leaf area
1076 index in a chemical transport model: Strength of feedback and implications for ozone air quality and vegetation health, *Atmos.*
1077 *Chem. Phys.*, doi:10.5194/acp-18-14133-2018, 2018.
- 1078 Zhu, Z., Bi, J., Pan, Y., Ganguly, S., Anav, A., Xu, L., Samanta, A., Piao, S., Nemani, R. R. and Myneni, R. B.: Global data
1079 sets of vegetation leaf area index (LAI)_{3g} and fraction of photosynthetically active radiation (FPAR)_{3g} derived from global



1080 inventory modeling and mapping studies (GIMMS) normalized difference vegetation index (NDVI3G) for the period 1981 to
1081 2, *Remote Sens.*, doi:10.3390/rs5020927, 2013.

1082 Zhu, Z., Piao, S., Myneni, R. B., Huang, M., Zeng, Z., Canadell, J. G., Ciais, P., Sitch, S., Friedlingstein, P., Arneth, A., Cao,
1083 C., Cheng, L., Kato, E., Koven, C., Li, Y., Lian, X., Liu, Y., Liu, R., Mao, J., Pan, Y., Peng, S., Peñuelas, J., Poulter, B., Pugh,
1084 T. A. M., Stocker, B. D., Viovy, N., Wang, X., Wang, Y., Xiao, Z., Yang, H., Zaehle, S. and Zeng, N.: Greening of the Earth
1085 and its drivers, *Nat. Clim. Chang.*, 6(8), 791–795, doi:10.1038/nclimate3004, 2016.

1086

1087